

Classification of Disordered Phases of Quantum Hall Edge States

Joel E. Moore and Xiao-Gang Wen

Department of Physics, Massachusetts Institute of Technology, Cambridge, MA 02139

(October 20, 1997)

The effects of impurity scattering on a general Abelian fractional quantum Hall (FQH) edge state are analyzed within the chiral-Luttinger-liquid model of low-energy edge dynamics. We find that some disordered edges can have several different phases characterized by different symmetries. The stable impurity edge phases are in general more symmetric than the original clean system and demonstrate the phenomenon of dynamical symmetry restoration at low energies and long length scales. The phase transitions between different disordered phases are characterized by broken symmetries and obey Landau's symmetry breaking principle for continuous phase transitions. Phase diagrams for various edges are found using a new system of coordinates for the interactions between modes in a quantum Hall edge. The temperature dependence of tunneling through a point contact is calculated and is found to be able to distinguish different impurity edge phases of the same FQH state.

PACS numbers: 72.10.-d 73.20.Dx

I. INTRODUCTION

It was realized soon after the discovery of the integer quantum Hall effect (QHE) that interesting phenomena occur at the one-dimensional boundary of a two-dimensional electron gas.¹ In a strong applied magnetic field, the bulk electron gas forms an incompressible quantum liquid² at certain filling factors ν which are found experimentally to be either integers or simple fractions. The only gapless excitations at these filling factors are along the edge of the liquid and as a result current flow is confined to the edge.³ The low-energy excitation spectrum at the edge is accessible to tunneling⁴ and magnetoplasma⁵ experiments and in principle allows the structure of complicated FQH liquids to be probed because of the connection between the internal topological orders of the bulk electron gas^{6,7} and the "chiral Luttinger liquid" theory of the edge.⁸

The properties of disordered quantum Hall edges are important for a number of reasons. The edge is described by a chiral Luttinger liquid (χ LL) theory similar to the ordinary Luttinger liquid,⁹ the generic state of a one-dimensional interacting electron gas, which is known to be sensitive to impurities. In fact, the difficulty involved in fabricating sufficiently clean and conducting one-dimensional electron gases has led to interest in quantum Hall edges as an ideal one-dimensional system.¹⁰ The quantum Hall edge can be impervious to disorder, as in the $\nu = 1$ state, which has a single branch of low-energy excitations propagating in one direction and hence remains conducting when random impurities are added.

The effects of disorder on a nonchiral Hall edge (one with excitations moving in both directions) are more complex. The χ LL theory of a clean edge with n condensates is characterized by two matrices K and V and a charge vector \mathbf{t} : the K matrix describes the topological orders of the bulk state, such as the relative statistics of quasiparticles, and the V matrix gives the edge Hamil-

tonian and related properties such as velocities. K is taken to be the same for all edges of the same quantum Hall state, while the values in V are nonuniversal and expected to vary for different experiments. The conductance of a maximally chiral edge (all modes propagating in the same direction) is independent of V and hence universal. For clean nonchiral edges, the conductance calculated using the Kubo formula depends on V and thus appears to be nonuniversal, contradicting experiment. The conductance is bounded below by the quantized value $\nu e^2/h$ associated with the bulk filling factor ν but only has this value for a subset of the allowed V matrices. However, in real samples, the different modes at the edge equilibrate and the conductance takes the quantized value. Kane, Fisher, and Polchinski (KFP) argued that for the $\nu = 2/3$ edge this equilibration is caused by scattering from random impurities.¹¹

Haldane has argued that an additional term must be included in the Kubo conductance formula to account for contributions from the bulk QHE liquid.¹² With this term the conductance is always fixed at the quantized value $\nu e^2/h$, even for a nonchiral edge. This argument involves some subtle questions which have been partly explored in later work;¹³ here we will just mention that disorder-driven instabilities can affect other measurable properties besides the conductance, such as tunneling behavior through a point contact. Thus such instabilities are relevant to experiments whether or not the original use of the Kubo formula is correct. One result of our work is that for some edges measurably different phases can occur even when the conductance, calculated with or without the additional term, is fixed at the quantized value.

The equilibration of different edge modes is also an important process in the integer quantum Hall effect with $\nu = n$, since nonideal contacts will populate the n different edge channels at different chemical potentials. Inter-channel electron scattering can equilibrate the modes, as predicted by Büttiker¹⁴ and demonstrated in several in-

novative experiments.^{15–17} Experiments show equilibration in the IQHE on a length scale $\ell_e \sim 40 \mu\text{m}$. Nonchiral FQH edges differ in that even ideal contacts do not give rise to an equilibrated edge. Some interactions capable of transferring charge between channels, such as backscattering by random impurities and/or electron-phonon interactions, are necessary for edge equilibration.¹³ In real samples the different branches of FQH edges are always close to each other and the different branches are always in equilibrium, which leads to a quantized Hall conductance.

The $\nu = 2/3$ edge contains one branch propagating in each direction. KFP showed that when impurity scattering is relevant, it can drive the velocity matrix V to one of the subset of possible values which give conductance quantization. This subset of “charge-unmixed” V matrices has a simple physical property: one eigenmode of edge fluctuation is charged and the others are neutral, with no interaction between the charged and neutral eigenmodes. Impurity scattering is not relevant for every velocity matrix, so conductance may not always be quantized. But for all velocity matrices sufficiently close to a charge-unmixed matrix, weak impurity scattering drives the edge state to the fixed point, where the velocity matrix is charge-unmixed and the conductance is quantized.

The V matrices for current experimental setups may all fall within the basin of attraction of the KFP fixed point. A velocity matrix is close to a charge-unmixed matrix if the interaction between charged modes has much higher energy than the interaction between a charged mode and a neutral mode. The Coulomb interaction between charges in an experimental QHE setup is typically only screened at a distance of many magnetic lengths $\ell = \sqrt{\hbar c/eB}$ from the edge, so that the charge-charge interaction may indeed be much larger than the residual interaction between a charged mode and a neutral one.¹⁸

The flow to the impurity fixed point is especially interesting from the point of view of symmetries of the χLL action. The K matrix of the state $\nu = n/(2n - 1)$ has a hidden $SU(n)$ symmetry, as first pointed out by Read.¹⁹ A generic V matrix breaks the symmetry of the K matrix, but precisely at the impurity fixed point, the velocity matrix does have all the symmetries of K .²⁰ The impurity scattering thus acts to *increase* the symmetry of the edge. In this paper we find that in some quantum Hall edges the impurity fixed points have some but not all of the symmetries of the K matrix. In this case different fixed points are related by symmetry transformations, in the same way as the spin-up and spin-down fixed points of the Ising ferromagnet in zero external field are different but are related by a symmetry of the starting Hamiltonian. This new type of broken symmetry is discussed in Section IV. Edge states differ from ferromagnets in that symmetry is “spontaneously restored” rather than spontaneously broken: a starting Hamiltonian of low symmetry is driven by impurity scattering to a more symmetric fixed point.

In this article we analyze the effects of impurity scattering on a general nonchiral quantum Hall edge. Not all edge states have a potentially relevant impurity scattering operator, which is required for impurity scattering to cause edge equilibration. For example, it is shown in Section III that the only nonchiral level two states in the Haldane-Halperin hierarchy^{21,22} with a possibly relevant impurity scattering operator are the principal hierarchy states with filling factor $\nu = 2/(2p + 1)$, p an odd integer. The other level two states, such as $\nu = 4/5$, have an equilibration length from impurity scattering which diverges at low temperature.¹³ Edges with no relevant operators may still equilibrate by another process such as inelastic scattering from phonons. In order to determine whether a given state flows to an impurity fixed point, it is necessary to consider all the potentially relevant scattering operators in the chiral Luttinger liquid theory.

Section II defines a function $K(\mathbf{m})$ whose absolute value is twice the minimum scaling dimension of the vertex operator $O_{\mathbf{m}} = \exp(i \sum_j m_j \phi_j)$, where the m_j are integers and ϕ_j are the fields of the χLL theory. For impurity scattering $O_{\mathbf{m}}$ has charge zero and $K(\mathbf{m})$ is an even integer. Impurity scattering operators with $|K(\mathbf{m})| \geq 4$ are never relevant. Equilibration by impurity scattering depends on having scattering operators with $|K(\mathbf{m})| = 2$ to drive the velocity matrix to a charge-unmixed matrix. Haldane has argued that a neutral operator $O_{\mathbf{m}}$ with $K(\mathbf{m}) = 0$ drives a topological instability which removes a pair of oppositely directed neutral modes from the low-energy theory.¹² Edges with no neutral $K(\mathbf{m}) = 0$ operators are “ T -stable” and it is conjectured that only T -stable states are seen experimentally. All the examples studied in this paper are T -stable, but the methods introduced do not depend on T -stability.

T -stability is useful because there are only finitely many classes of T -stable states with neutral modes in both directions, as we now explain. In Section II we introduce a system of coordinates for the V matrix which simplifies the treatment of states with several condensates. The dimension of the coordinate space is less than the number of free parameters in V . For states with all neutral modes traveling opposite to the charge mode, the charge-unmixed subset is a single point in these coordinates and a small number of $|K(\mathbf{m})| = 2$ operators are relevant in a region around this point, which is the only impurity fixed point. This class includes the $\nu = n/(2n - 1)$ states. For $\dim K = 3$ there are also states in which the charge-unmixed matrices form a line in our coordinate space and there are infinitely many $|K(\mathbf{m})| = 2$ operators. These states have many impurity fixed points. With $\dim K = 4$ the charge-unmixed states can form a plane or a point. For $\dim K = 5$ there are no principal hierarchy states and for $\dim K > 5$ no states at all which are T -stable and have neutral modes moving in both directions, as a consequence of a deep theorem on integral quadratic forms.^{12,23}

Section III studies T -stable hierarchical quantum Hall states and finds that several classes of such states ex-

hibit “ V stability”: every V matrix sufficiently close to a charge-unmixed matrix is driven to a charge-unmixed matrix by weak impurity scattering. In particular, every principal hierarchy state with two or three condensates is shown to have this property. Some of the three-species states have infinitely many possibly relevant operators which lead to many impurity fixed points with different charge-unmixed V matrices. For V stable states, impurity scattering can explain the edge equilibration and robust quantization seen experimentally.

The rest of this article is organized as follows. Section II puts the model of a general Abelian quantum Hall edge with impurities into a form which isolates the dependence of scaling dimensions of various operators on the velocity matrix. This is convenient for the calculation of phase diagrams for particular edges in Section III. Section III applies the formalism to states in the hierarchy containing several species of quasiparticles and finds new behaviors associated with the existence of a large number of possibly relevant operators. Two classes of edges with high symmetry are studied in some detail: the $SU(n) \times U(1)$ edge solved exactly by Kane and Fisher²⁰ and the “Fibonacci” edge, in which the sequence $a_{n+1} = a_n + a_{n-1}$ plays a special role. All principal hierarchy states with three condensates are shown to belong to one of these two classes. The Fibonacci edge has two types of fixed points which correspond to different phases with different tunneling conductance and other measurable properties. Some four-condensate edges, such as $\nu = 12/17$, are shown to have three different types of fixed points, representing three different broken symmetries of the K matrix.

Sections IV-VI contain results obtained using the method developed in the earlier, more technical sections and require only a general understanding of the earlier sections. Section IV explains how the many fixed points in some edges are related to broken symmetries of the K matrix. Section V examines the experimental consequences of the multiple phases in disordered edges. The low-temperature scaling behavior of the tunneling conductance through a point constriction is calculated for all phases of all T -stable principal hierarchy states with filling fractions $\nu > 1/4$. This experiment is capable of distinguishing different impurity phases of the same edge state. In Section VI we summarize our results from the point of view of general principles of phase transitions.

II. GENERAL PROPERTIES OF THE DISORDERED EDGE

Edges of quantum Hall systems are described by a chiral Luttinger liquid (χ LL) theory related to the topological orders of the bulk quantum Hall state. We introduce the theory for a clean edge and diagonalize it to obtain scaling dimensions of impurity scattering operators. The χ LL action in imaginary time for a clean edge of a QH

state characterized by the matrix K contains $n = \dim K$ bosonic fields ϕ_i and has the form⁸

$$S_0 = \frac{1}{4\pi} \int dx d\tau [K_{ij} \partial_x \phi_i \partial_\tau \phi_j + V_{ij} \partial_x \phi_i \partial_x \phi_j] \quad (2.1)$$

where, as in the rest of this paper, the sum over repeated indices is assumed. K is a symmetric integer matrix and V a symmetric positive matrix. K gives the topological properties of the edge: the types of quasiparticles and their relative statistics. V , the velocity matrix, is positive definite so that the Hamiltonian is bounded below. The charges of quasiparticles are specified by an integer vector \mathbf{t} and the filling factor is $\nu = t_i (K^{-1})_{ij} t_j$.

Scattering by spatially random quenched impurities is described by the action

$$S_1 = \int dx d\tau [\xi(x) e^{im_j \phi_j} + \xi^*(x) e^{-im_j \phi_j}] \quad (2.2)$$

Here ξ is a complex random variable and $[\xi(x)\xi^*(x')] = D\delta(x-x')$, with D the (real) disorder strength. The integer vector \mathbf{m} describes how many of each type of quasiparticle are annihilated or created by the operator $O_{\mathbf{m}} = \exp(im_j \phi_j)$. For a real system all charge-neutral scattering operators m_j are expected to appear, but most of these will be irrelevant in the RG sense as discussed in the following. The condition for charge-neutrality is $t_i (K^{-1})_{ij} m_j = 0$. The random variables $\xi_{\mathbf{m}}$ for different scattering operators $O_{\mathbf{m}}$ may be uncorrelated or correlated depending on the nature of the physical impurities causing the scattering.

Now consider the correlation functions of these scattering operators with respect to the clean action S_0 . For integer vectors \mathbf{m} , define the function $K(\mathbf{m}) \equiv m_i (K^{-1})_{ij} m_j$. $K(\mathbf{m})$ governs the topological part of the correlation function of the scattering operator $O_{\mathbf{m}}$ as follows: the correlation function is, ignoring cutoffs,

$$G(x, \tau) = \langle e^{im_j \phi_j(x, \tau)} e^{-im_j \phi_j(0, 0)} \rangle \propto (\prod_{k=1}^{n^+} (x + iv_k^+ \tau)^{-\alpha_k}) (\prod_{k=1}^{n^-} (x - iv_k^- \tau)^{-\beta_k}). \quad (2.3)$$

Here n^+ and n^- are the numbers of positive and negative eigenvalues of K , and $v_k^\pm, \alpha_k, \beta_k$ are nonnegative real numbers which depend on V and K . However, $\sum_{k=1}^{n^+} \alpha_k - \sum_{k=1}^{n^-} \beta_k = K(\mathbf{m})$ independent of V . Setting all velocities $v_k^\pm = 1$ and introducing $z = x + i\tau$,

$$\langle e^{im_j \phi_j(x, \tau)} e^{-im_j \phi_j(0, 0)} \rangle \propto \frac{1}{z^{K(\mathbf{m})}} \frac{1}{|z|^{2\Delta(\mathbf{m}) - K(\mathbf{m})}} \quad (2.4)$$

with $K(\mathbf{m})$ assumed positive. $\Delta(\mathbf{m}) = (\sum_{k=1}^{n^+} \alpha_k + \sum_{k=1}^{n^-} \beta_k)/2$ is the scaling dimension of the operator $\exp(im_j \phi_j)$.

The scaling dimensions of the various operators in the theory are functions of V , an $n \times n$ matrix. Much of the physics of a disordered edge depends on V only through

the scaling dimensions of various operators. The conductance in units of e^2/h is given by twice the scaling dimension $\Delta(\mathbf{t})$ of the charge operator as a consequence of the Kubo formula.¹¹ This is the conductance measured with ideal contacts; a kinetic theory model for nonideal tunnel-junction contacts gives a different nonuniversal value.¹³ It remains true that edge equilibrium is required for the universal value of conductance $\nu e^2/h$ to be observed, and a necessary condition is $2\Delta(\mathbf{t}) = \nu$.

The scaling dimension of an operator determines whether that operator is relevant in the RG sense when added to the clean action S_0 . The operator is relevant with a uniform coefficient when $\Delta(\mathbf{m}) < 2$, relevant with a spatially random coefficient when $\Delta(\mathbf{m}) < 3/2$, and relevant at a point (with a δ -function coefficient) when $\Delta(\mathbf{m}) < 1$. For the random case this follows from the leading-order RG flow equation for disorder strength D ,²⁴

$$\frac{dD}{dl} = (3 - 2\Delta)D. \quad (2.5)$$

It is thus useful to write V in a way which isolates the parts of V which affect $\Delta(\mathbf{m})$ so that scaling dimensions depend on as few parameters as possible.

Equation 2.3 is obtained by simultaneously diagonalizing K and V by a basis change $\phi_i = M_{ij}\tilde{\phi}_j$. Suppose M_1 brings K to the pseudo-identity $I(n^+, n^-)$, i.e.,

$$M_1^T K M_1 = I_{n^+, n^-} = \begin{pmatrix} I_{n^+} & 0 \\ 0 & -I_{n^-} \end{pmatrix}. \quad (2.6)$$

Basis changes preserve the number of positive and negative eigenvalues of a matrix ("Sylvester's law of inertia"). Now consider another basis change M_2 which will diagonalize V without affecting the pseudo-identity: $M_2 \in SO(n^+, n^-) \Rightarrow M_2^T I(n^+, n^-) M_2 = I(n^+, n^-)$, introducing the proper pseudo-orthogonal group $SO(m, n)$. The real positive symmetric matrix $V' \equiv M_1^T V M_1$ can be written as $(M_2^{-1})^T V_D M_2^{-1}$ for some diagonal matrix V_D and some $M_2 \in SO(n^+, n^-)$. The entries in V_D are all positive and are the v_k^\pm from (2.3), with (v^+, v^-) corresponding to (positive, negative) eigenvalues of K .

Since V_D and $I(n^+, n^-)$ are diagonal, the correlation functions in the basis $\tilde{\phi} = (M_1 M_2)^{-1} \phi$ are trivial:

$$\begin{aligned} \langle e^{i\tilde{\phi}_j(x, \tau)} e^{-i\tilde{\phi}_j(0, 0)} \rangle &= e^{\langle \tilde{\phi}_j(x, \tau) \tilde{\phi}_j(0, 0) \rangle - \langle \tilde{\phi}_j(0, 0) \tilde{\phi}_j(0, 0) \rangle} \\ &\propto \frac{1}{x \pm i v_j \tau} \end{aligned} \quad (2.7)$$

where the sign depends on whether $\tilde{\phi}_j$ appears with -1 or $+1$ in $I(n^+, n^-)$. Going back to the original fields ϕ , we obtain

$$K^{-1} = M_1 M_2 I_{n^+, n^-} M_2^T M_1^T = M_1 I_{n^+, n^-} M_1^T, \quad (2.8)$$

$$V_D = M_2^T M_1^T V M_1 M_2. \quad (2.9)$$

Let us define a matrix Δ through

$$\begin{aligned} I &= M_2^T M_1^T (2\Delta)^{-1} M_1 M_2 \\ \Rightarrow 2\Delta &= M_1 M_2 M_2^T M_1^T. \end{aligned} \quad (2.10)$$

The positive definite matrix Δ gives the scaling dimension of the operator $O_{\mathbf{m}}$: $\Delta(\mathbf{m}) = m_i \Delta_{ij} m_j$. Note that under the basis change $\phi_i = M_{ij}\tilde{\phi}_j$, the vector \mathbf{m} transforms to preserve $\tilde{m}_i \tilde{\phi}_i = m_i \phi_i = m_i M_{ij} \tilde{\phi}_j$, so $\tilde{\mathbf{m}} = M^T \mathbf{m}$. Thus the functions $K(\mathbf{m})$ and $\Delta(\mathbf{m})$ are basis-invariant.

The scaling dimensions are independent of the $n = n^+ + n^-$ velocities in V_D , as expected on physical grounds. M_1 depends only on K , not on V , so all possible matrices Δ for a given edge are obtained as M_2 ranges over $SO(m, n)$ with M_1 fixed. We now introduce a parameterization of M_2 in which only $n^+ n^-$ coordinates affect Δ . The physical picture is that the scaling dimensions are independent of the velocities of the eigenmodes and also of the interactions between modes going in the same direction; the scaling dimensions are only affected by interactions between counterpropagating modes. Thus of the $n(n+1)/2$ free parameters in V , n correspond to velocities of eigenmodes, $(n^+(n^+ - 1) + n^-(n^- - 1))/2$ to same-direction interactions, and $n^+ n^-$ to opposite-direction interactions.

The study of a nonchiral edge with several branches of excitations is thus feasible if one is willing to concentrate on edge properties and renormalization-group flows determined by the scaling dimensions of various operators. There are interesting physical phenomena which are not determined solely by scaling dimensions, such as the equilibration of velocities of modes moving in the same direction by interchannel hopping (which does not affect the conductance). But the effects of disorder on the commonly measured physical properties can be obtained from studying only the $n^+ n^-$ parameters of V which affect scaling dimensions, rather than the $n(n+1)/2$ needed for a complete description of the theory. This is apparent in the study of an $n = 2$ case ($\nu = 2/3$)¹¹: the velocity matrix has the form

$$V = \begin{pmatrix} v_1 & v_{12} \\ v_{12} & 3v_2 \end{pmatrix} \quad (2.11)$$

with one branch in each direction, and the conductance and the structure of the RG flow are found to depend only on the combination $c = 2v_{12}(v_1 + v_2)^{-1}/\sqrt{3}$.

The separation of V comes about because every element M in $SO(m, n)$ can be written as a product of a symmetric positive matrix B and an orthogonal matrix R , both of which are in $SO(m, n)$. This is a generalization of the familiar decomposition of a Lorentz transformation (an element of $SO(3, 1)$) into a boost (a symmetric positive matrix) and a rotation (an orthogonal matrix). For all examples in this paper $m = 1$ or $n = 1$ and this decomposition follows easily from the parameterization of boost matrices given below. More details are in Appendix A. Writing $M_2 = BR$,

$$2\Delta = M_1 M_2 M_2^T M_1^T = M_1 B R R^T B^T M_1^T = M_1 B^2 M_1^T. \quad (2.12)$$

So Δ is independent of R and depends only on the $n^+ n^-$ parameters in B . B can be written

$$B = \exp \begin{pmatrix} \mathbf{0} & b \\ b^T & \mathbf{0} \end{pmatrix} \quad (2.13)$$

for some $n^+ \times n^-$ matrix b .

For a maximally chiral edge, the boost part B is just the identity matrix, so the scaling dimension of every operator $\exp(im_j \phi_j)$ is independent of V , and in particular the conductance $\sigma = 2\Delta(t) = K(t) = \nu$. For nonchiral edges, nonuniversal values of the conductance are possible with $2\Delta(t) \geq \nu$ and equality if and only if the velocity matrix is charge-unmixed. This is a special case of the general property $2\Delta(\mathbf{m}) \geq |K(\mathbf{m})|$ for all integer vectors \mathbf{m} (with equality if and only if the V_{1j} vanish in the basis with $\mathbf{e}_1 \parallel \mathbf{m}$ and K^{-1} diagonal). Consequently the scattering term $\exp(im_j \phi_j)$ can only be relevant if $|K(\mathbf{m})| \leq 3$. The scattering operator must have bosonic commutation relations so the three possibilities are $K(\mathbf{m}) = 2, 0, -2$. If a null vector exists with $K(\mathbf{m}) = 0$, the edge is not T -stable. Operators with $|K(\mathbf{m})| = \pm 2$ are necessary if the impurities are to drive the edge state to a fixed point. The next step is to calculate which velocity matrices make the scattering terms $\xi(x) \exp(im_j \phi_j) + \xi^*(x) \exp(-im_j \phi_j)$ relevant.

The possible matrices Δ for a given edge can be studied simply by calculating $2\Delta = M_1 B^2 M_1^T$ for all boosts B . For a two-component edge with one branch propagating in each direction, there is just one boost parameter. For a three-component edge, there are two parameters, and the scaling dimensions of various operators can be plotted on the plane as functions of these two parameters. For $SO(1, m)$ a useful parameterization of boosts as a function of momentum coordinates (p_1, \dots, p_m) is²⁵

$$B_{11} = \gamma = \sqrt{1 + p^2}, \quad B_{1i} = B_{i1} = p_{i-1}, \\ B_{ij} = \delta_{ij} + p_{i-1} p_{j-1} (\gamma - 1) / p^2 \quad (2.14)$$

where $2 \leq i, j \leq m+1$. It is convenient to work with dimensionless momentum $\mathbf{p} = \gamma \mathbf{v}$ because of the singularity at $v = c = 1$ in the velocity coordinates. However, in Section III we mention an advantage of the velocity coordinates for certain edges. Permuting indices gives a version appropriate for $SO(m, 1)$.

For a given edge it is now possible to search for all possibly relevant neutral operators ($|K(\mathbf{m})| = 2$) and then calculate where in the space of boost parameters each operator is relevant. The rest of this section describes a few technical details needed to carry out this program. The search for $|K(\mathbf{m})| = 2$ operators is done on a computer: there is a finite p-adic test for whether an integer quadratic form takes the value zero,²³ but we know of none to determine all vectors for which an integer quadratic form takes a particular nonzero value. When

finding phase diagrams in the next section, it will be useful to consider basis changes not in $SL(n, Z)$ which bring K^{-1} to diagonal form, so that the locality condition is no longer that \mathbf{m} be an integer vector. The local operators in the new theory are the transforms of integer vectors in the original theory. The advantage of such a basis change $K^{-1} \rightarrow OK^{-1}O^T$, $\mathbf{m} \rightarrow O^T \mathbf{m}$ which makes K^{-1} diagonal and brings the charge vector \mathbf{t} to the first basis vector \mathbf{e}_1 is that some of the boost parameters can be interpreted as the strength of mixing of the charge mode with neutral modes. Then the charge-unmixed velocity matrices will be exactly those with these boost parameters equal to zero. Table I summarizes the possible parameter spaces for all nonchiral edges with four or fewer components.

For each operator with $|K(\mathbf{m})| = 2$, there is some velocity matrix which gives that operator scaling dimension $2\Delta(\mathbf{m}) = 2$: this follows from the possibility of choosing M_1 in (2.8-2.10) to make \mathbf{m} one of the basis vectors and choosing M_2 so that all parameters rotating \mathbf{m} into other basis vectors are zero. The operation of changing bases distorts the phase diagram nonlinearly but preserves its topology and produces the same set of possible scaling matrices Δ . The sign of $K(\mathbf{m})$ will turn out to affect the dimension of the subset of matrices V which make $\exp(im_j \phi_j)$ maximally relevant. The examples of different types of edges listed in Table I are the subject of the following section.

III. STRUCTURE OF DISORDERED EDGES

The method described in the previous section greatly simplifies the analysis of a nonchiral edge of several condensates. In particular it allows us to determine in which regions of the space of velocity matrices V a particular impurity scattering operator $\exp(im_j \phi_j)$ is relevant, and hence determine the phase diagram of the edge state. We find that the edge of a single quantum Hall state can have different phases, with transitions between phases caused by changes in V . We also find that only a special class of edge states (“principal hierarchy states”) have enough $|K(\mathbf{m})| = 2$ impurity scattering operators to ensure that the conductivity is driven to the quantized value. The phase diagrams for this class of edge states show remarkable symmetries absent in the phase diagram of a general edge. In Section IV these symmetries are shown to reflect broken symmetries of the K matrix.

All the examples are in the hierarchy of quantum Hall states.^{21,22} Hierarchical states have tridiagonal K matrices with all off-diagonal matrix elements equal to 1 and $K_{11} = l$ an odd integer, $K_{ii} = n_i$ even for $i = 2, \dots, \dim K$. The matrix will often be given simply by its diagonal elements (l, n_2, \dots) . The charge vector is $\mathbf{t} = (1, 0, \dots, 0)$. The number of modes moving opposite the direction of the charge mode is equal to the number of negative elements on the main diagonal. States with

all $|n_i| = 2$ are called principal states and are the most stable states at each level of the hierarchy.

First we study the edges of all hierarchy states at second level ($\dim K = 2$) and show that the principal hierarchy states are all similar to the $\nu = 2/3$ state studied by KFP. The states which are not principal have no relevant random operators and are thus unaffected by weak impurity scattering. In particular, for these states elastic impurity scattering alone is insufficient to give edge equilibration at low temperature.

A rich variety of behavior is possible for $\dim K = 3$ states, where the two neutral modes can move in the same direction (opposite the charge mode) or in opposite directions (cf. Table I). The principal hierarchy state of $\dim K = n$ with all neutral modes in the same direction flows to an $SU(n) \times U(1)$ fixed point which is the only point where conductance is quantized. The charge mode satisfies a $U(1)$ Kac-Moody algebra, and the $n-1$ neutral modes satisfy an $SU(n)$ Kac-Moody algebra. The highly symmetric phase diagram for the $SU(3)$ case is shown not to describe the simplest few non-principal states.

For the $\dim K = 3$ case with neutral modes in both directions, conductance is quantized along a line in the phase diagram, and for the principal hierarchy states we find an infinite number of fixed points along this line corresponding to the infinite number of possibly relevant random operators. There are two different types of fixed points which correspond to two measurably different phases. A few results on the $\dim K = 4$ cases are also presented. No principal hierarchy edges with $\dim K > 4$ are topologically stable except those with all neutral modes in the same direction.¹²

A. Edges with $\dim K = 2$

The K matrix in the hierarchy basis has the form

$$K = \begin{pmatrix} l & 1 \\ 1 & n \end{pmatrix}, \quad \mathbf{t} = (1, 0) \quad (3.1)$$

with l odd and n even. For the state to be nonchiral, $n < 0$. A quick calculation shows that if $\mathbf{m} = (m_1, m_2)$ is a charge-neutral $K(\mathbf{m}) = -2$ operator (there are no charge-neutral $K(\mathbf{m}) = 2$ operators), $m_1^2 = -2/n$ which has the solutions $m_1 = \pm 1$ if $n = -2$ and no integer solution otherwise. Hence for principal hierarchy states ($n = -2$) there is one complex-conjugate pair of possibly relevant operators labeled by $\mathbf{m} = \pm(1, -2)$, while for other hierarchy states there are no relevant random operators.

For a $\dim K = 2$ state there is a single boost parameter p and a single value of this parameter that makes V charge-unmixed. It remains to show that this value is exactly the value which gives the scattering operator $\exp(im_j \phi_j)$ its minimum scaling dimension $\Delta = 1$. In the basis of $\mathbf{t} = (1, 0)$ and $\mathbf{m} = (1, -2)$, K^{-1} is diagonal

with elements $(\nu, -2)$ and the scaling dimension matrix is

$$\begin{aligned} 2\Delta &= \begin{pmatrix} \sqrt{\nu} & 0 \\ 0 & \sqrt{2} \end{pmatrix} B^2 \begin{pmatrix} \sqrt{\nu} & 0 \\ 0 & \sqrt{2} \end{pmatrix} \\ &= \begin{pmatrix} \sqrt{\nu} & 0 \\ 0 & \sqrt{2} \end{pmatrix} \begin{pmatrix} \sqrt{1+p^2} & p \\ p & \sqrt{1+p^2} \end{pmatrix} \begin{pmatrix} \sqrt{\nu} & 0 \\ 0 & \sqrt{2} \end{pmatrix}. \end{aligned} \quad (3.2)$$

The conductance $2\Delta(t)$ is $\nu\sqrt{1+p^2}$ and the scaling dimension $\Delta(\mathbf{m})$ is $\sqrt{1+p^2}$. So $\Delta(\mathbf{m}) = 1$ exactly at the charge-unmixed point ($p = 0$), as required. The region of attraction of this fixed point is determined by the equation $\Delta(\mathbf{m}) \leq 3/2$ giving $-\sqrt{5}/2 \leq p \leq \sqrt{5}/2$ for $\nu = 2/3$.

Now we briefly outline the exact solution at the fixed point found by KFP which also shows the stability of the fixed point under RG transformations. Let the elementary fields in the basis defined above be the charge mode ϕ_ρ and neutral mode ϕ_σ . At the fixed point,

$$K = \begin{pmatrix} \nu & 0 \\ 0 & -2 \end{pmatrix}, \quad V = \begin{pmatrix} v_\rho & 0 \\ 0 & 2v_\sigma \end{pmatrix}. \quad (3.3)$$

The three operators $\partial_x \phi_\sigma, \exp(i\phi_\sigma), \exp(-i\phi_\sigma)$ all have scaling dimension 1 and satisfy an $SU(2)$ algebra. The action at the fixed point is

$$\begin{aligned} S &= \int_{x,\tau} \left[\frac{\nu \partial_x \phi_\rho}{4\pi} (i\partial_\tau + v_\rho \partial_x) \phi_\rho \right. \\ &\quad \left. + \frac{2\partial_x \phi_\sigma}{4\pi} (-i\partial_\tau + v_\sigma \partial_x) \phi_\sigma + (\xi(x)e^{i\phi_\sigma} + \text{h.c.}) \right], \end{aligned} \quad (3.4)$$

obtained by substituting the fixed point K and V into (2.1,2.2). Now the fixed point action can be written in terms of a two-component Fermi field by introducing an auxiliary bosonic field χ which does not affect physical quantities: $\psi_1 = \exp[i(\chi + \phi_\sigma)/\sqrt{2}]$, $\psi_2 = \exp[i(\chi - \phi_\sigma)/\sqrt{2}]$. The clean part of the action is diagonal in the components while the impurity term becomes a hermitian combination of raising and lowering operators, $\psi_1^\dagger \psi_2$ and $\psi_2^\dagger \psi_1$, with random coefficients. The impurity term is then eliminated by a local $SU(2)$ gauge transformation which preserves the clean part of the action. The clean part of the action is just the action for free chiral fermions.

When the system is near but not at the fixed point, there is a weak coupling $V_{\rho\sigma} \partial_x \phi_\rho \partial_x \phi_\sigma$ between the charged and neutral modes. The scaling dimension of this term in the original action is 2 so the operator is marginal with a uniform coefficient. However, the $SU(2)$ rotation of $\partial_x \phi_\sigma$ gives this term a random coefficient and makes it irrelevant. According to this picture, once V falls into the basin of attraction of the fixed point, i.e., $|p| \leq \sqrt{5}/2$ in (3.2), it flows to the fixed point $p = 0$ with K and V given by (3.3). Since the boost part of V is uniquely determined at the fixed point, many physical properties are uniquely determined, such as the conductance $\sigma = \nu e^2/h$. The same technique of fermionization followed by a gauge transformation solves the $SU(n) \times U(1)$ fixed point described below.

B. Three-branch edges with parallel neutral modes

Such edges have both neutral modes antiparallel to the charge mode (line 3 of Table I). There is a single charge-unmixed point in the boost coordinates of Section II. In the hierarchy representation such edges have K matrix $(l, -n_1, -n_2)$. The principal hierarchy edges of this type are $\nu = 3/5$ with $K = (1, -2, -2)$, $\nu = 3/11$ with $K = (3, -2, -2)$, and so forth. The principal hierarchy edges with n condensates and all neutral modes antiparallel to the charge mode have an $SU(n)$ symmetry ($n = \dim K$) in their K matrix $(l, -2, \dots, -2)$, as first pointed out by Read.¹⁹ The filling fraction is $\nu = n/(n(l+1) - 1)$. Kane and Fisher showed²⁰ that each of these edges has a fixed point with a charge field ϕ_ρ of dimension $\nu/2$ and a set of $n-1$ dimension 1 neutral fields ϕ_σ^i obeying an $SU(n)$ algebra. There are $n-1$ roots of $SU(n)$ which correspond to the $n-1$ operators $\partial_x \phi_\sigma^i$. Now we obtain the phase diagram for the $n=3$ case, which is easily generalized to $n > 3$.

Any neutral operator $O_{\mathbf{m}}$ for these edges has negative $K(\mathbf{m})$ because all neutral modes travel opposite the direction of charge. There must be $(n^2 - 1) - (n - 1) = n(n - 1)$ operators with $K(\mathbf{m}) = -2$ in order to obtain the complete $SU(n)$ algebra (here \mathbf{m} and $-\mathbf{m}$ are counted independently). For $\nu = 3/5$ this requires 6 such operators which in the hierarchy basis are labeled by $\mathbf{m} = \pm(0, 1, -2), \pm(1, -2, 1), \pm(1, -1, -1)$. Now the technique of Section II can be used to find when these operators become relevant and thus the region of attraction of the fixed point. For this case the procedure is described in detail for the sake of clarity; for subsequent cases some intermediate steps will be skipped.

The basis $\{(1, 0, 0), (0, 1, -2), (2, -3, 0)\}$ brings K^{-1} to diagonal form with elements $(3/5, -2, -6)$. The above six operators with $K(\mathbf{m}) = -2$ become $\pm(0, 1, 0), \pm(0, 1/2, 1/2), \pm(0, 1/2, -1/2)$. At the fixed point point, V is also diagonal in the new basis $\{\phi_\rho, \phi_1, \phi_2\}$, and $\exp(i\phi_\rho)$ has scaling dimension $\nu/2 = 3/10$, $\exp(i\phi_1)$ scaling dimension 1, and $\exp(i\phi_2)$ scaling dimension 3, so that a neutral operator $\exp(im_1\phi_1 + im_2\phi_2)$ has scaling dimension $m_1^2 + 3m_2^2$. Let D be the diagonal matrix with diagonal elements $(\sqrt{3/5}, \sqrt{2}, \sqrt{6})$, which are the square roots of twice the scaling dimensions of the basis fields at the fixed point. Using the boost parameters (p_1, p_2) , $\gamma = \sqrt{1 + p_1^2 + p_2^2}$, to parameterize non-diagonal V , we find the scaling dimension matrix in the basis $\{\phi_\rho, \phi_1, \phi_2\}$ is

$$2\Delta = D \begin{pmatrix} \gamma & p_1 & p_2 \\ p_1 & 1 + \frac{p_1^2(\gamma-1)}{p_1^2+p_2^2} & \frac{p_1 p_2(\gamma-1)}{p_1^2+p_2^2} \\ p_2 & \frac{p_1 p_2(\gamma-1)}{p_1^2+p_2^2} & 1 + \frac{p_2^2(\gamma-1)}{p_1^2+p_2^2} \end{pmatrix}^2 D \quad (3.5)$$

From this equation it is apparent that for $p_1 = p_2 = 0$ (a diagonal V in the new basis) all six operators have scaling dimension equal to 1, and this is the only charge-unmixed point since if p_i is nonzero the charge mode is

partly mixed with the i th neutral mode. Fig. 1 shows the scaling dimension of the possibly relevant operators as functions of (p_1, p_2) . The scaling dimension of $(0, 1, 0)$ is independent of p_2 so its contours are exactly vertical. Note that such a plot can be drawn without any information about the fixed point.

The interpretation of RG flows from Fig. 1 is quite simple. Each relevant scattering operator causes the velocity matrix to move to make the operator maximally relevant ($\Delta = 1$). If the starting velocity matrix is near the origin, all three operators are relevant and drive the velocity matrix to the origin, the only point at which all three are maximally relevant. The high symmetry of the graph reflects the $SU(3)$ symmetry of the fixed point. General three-species hierarchy states do not have this symmetry in the phase diagram and do not have enough $|K(\mathbf{m})| = -2$ operators to determine a unique fixed point. For example, the $\nu = 7/11$ state $(1, -2, -4)$ and the $\nu = 7/9$ state $(1, -4, -2)$ both have just one $K(\mathbf{m}) = -2$ operator which is maximally relevant along a line through the origin. The phase diagram is like Fig. 1 with only one line instead of three. Now the charge-unmixed point has an $SU(2)$ symmetry rather than an $SU(3)$ symmetry because only one impurity operator is relevant. It is not clear that the system flows to this point in the absence of long-range interactions, even if it starts near the charge-unmixed point, because other points along the maximally relevant line are also possible fixed points.

The $\nu = 15/19$ state $(1, -4, -4)$ has no $|K(\mathbf{m})| = 2$ operators at all so no stable fixed points result from the addition of weak disorder. States with no $|K(\mathbf{m})| = 2$ operators are predicted to have diverging equilibration lengths from impurity scattering as temperature is lowered since impurity scattering is never relevant. For the other type of third level hierarchical states, which have one neutral mode parallel to the charge mode, the same basic property is seen: only for principal hierarchy states are there enough $|K(\mathbf{m})| = 2$ operators for impurity scattering to determine a discrete set of charge-unmixed fixed points.

C. Three-branch edges with antiparallel neutral modes

These edges have a line in the phase diagram along which the conductance is quantized, rather than a point as in the previous cases. For the principal hierarchy states, there are infinitely many $|K(\mathbf{m})| = 2$ operators, and these can be enumerated by a simple linear recursion relation. Examples are $\nu = 5/3$ with $K = (1, 2, -2)$, $\nu = 5/7$ with $K = (1, -2, 2)$, $\nu = 5/13$ with $K = (3, 2, -2)$, and $\nu = 5/17$ with $K = (3, -2, 2)$. These four edges all have the property that their $|K(\mathbf{m})| = 2$ operators $O_{\mathbf{m}}$ form a (vector) Fibonacci sequence: $\mathbf{m}_{n+1} = \mathbf{m}_n + \mathbf{m}_{n-1}$. The reason why these four edges have the same Fibonacci

pattern is that their χ LL theories have, up to a minus sign, the same neutral sector. Thus properties which depend only on neutral operators are shared by all states $K = (l, 2, -2)$ and $K = (l, -2, 2)$ independent of l . The familiar scalar Fibonacci sequence $(1, 1, 2, 3, 5, \dots)$ has previously appeared in physics in growth models of phyllotaxis. Note that the property $\mathbf{m}_{n+1} = \mathbf{m}_n + \mathbf{m}_{n-1}$ is linear and hence independent of basis.

The $\nu = 5/3$ edge is convenient to study because of its $SL(3, Z)$ equivalence to the diagonal K matrix with elements $(1, 1, -3)$. The charge vector in this basis is $\mathbf{t} = (1, 1, 1)$. This gives the state a natural interpretation as a $\nu = 1/3$ gas of holes in two filled Landau levels. Also in this basis $K(m_1, m_2, m_3) = K(m_2, m_1, m_3)$. The $|K(\mathbf{m})| = 2$ operators in this theory are labeled by $\mathbf{m} = \pm(1, -1, 0), \pm(1, 0, 3), \pm(2, -1, 3), \pm(3, -1, 6), \pm(5, -2, 9), \dots$ plus the same list with first and second elements exchanged. The sign of $K(\mathbf{m})$ alternates between terms in this sequence: $(1, -1, 0)$ has $K(\mathbf{m}) = 2$ (as befits hopping between two rightward-moving modes), $(1, 0, -3)$ has $K(\mathbf{m}) = -2$, and so forth. There is an important difference between $K(\mathbf{m}) = 2$ and $K(\mathbf{m}) = -2$ operators: $K(\mathbf{m}) = 2$ operators are maximally relevant along a line in the phase diagram, while $K(\mathbf{m}) = -2$ operators are maximally relevant at a single point. This happens for the same reason that the charge-unmixed region was a single point for edges with all neutral modes opposite the charge mode. In a basis with \mathbf{m} an eigenvector, if there are no other eigenvectors with the same direction then every boost involves \mathbf{m} and affects its scaling dimension. If there are other eigenvectors in the same direction, there is a nontrivial linear space of boosts which do not affect the scaling dimension of $O_{\mathbf{m}}$.

The scaling dimension of the first few $|K(\mathbf{m})| = 2$ operators for $\nu = 5/3$ are plotted in Fig. 2 as functions of boost parameters (p_n, p_c) according to

$$2\Delta = D' \begin{pmatrix} 1 + \frac{p_c^2(\gamma-1)}{p_c^2+p_n^2} & p_c & \frac{p_c p_n(\gamma-1)}{p_c^2+p_n^2} \\ p_c & \gamma & p_n \\ \frac{p_c p_n(\gamma-1)}{p_c^2+p_n^2} & p_n & 1 + \frac{p_n^2(\gamma-1)}{p_c^2+p_n^2} \end{pmatrix} D'. \quad (3.6)$$

This expression for Δ is in the basis $\mathbf{t} = (1, 1, 1)$, $\mathbf{m}_1 = (1, -1, 0)$ and $\mathbf{m}_2 = (1, 1, 6)$ in terms of the original basis. $\phi_\rho, \phi_1, \phi_2$ with $\phi_1 = (1, -1, 0), \phi_2 = (1, 1, 6)$ in terms of the original basis (where $K = (1, 1, -3)$). Let $\phi_\rho, \phi_1, \phi_2$ be the three boson fields in the new basis. The diagonal matrix D' has elements $(\sqrt{5/3}, \sqrt{2}, \sqrt{10})$. This expression for Δ is similar to (3.5) for $\nu = 3/5$ with two important differences: the scaling dimension of $e^{i\phi_2}$ is 5 rather than 3 at the fixed point ($p_n = p_c = 0$), and the timelike row and column of the boost matrix correspond to ϕ_1 rather than ϕ_ρ , because now it is one of the neutral modes rather than the charge mode which has no other modes parallel to it.

In the coordinate space (p_n, p_c) (Fig. 2), $K(\mathbf{m}) = -2$ operators are relevant on compact regions and $K(\mathbf{m}) = 2$ operators on noncompact regions of the plane. The fixed

points form lines and isolated points in Fig. 2, where one operator with $|K(\mathbf{m})| = 2$ is maximally relevant. For fixed points on the charge-unmixed line $p_c = 0$ (the x -axis in Fig. 2), there are two marginal operators with the opposite sign of $K(\mathbf{m})$. The x -coordinates of these special points are found by taking alternately the rational part and the coefficient of $\sqrt{5}$ in $((1 + \sqrt{5})/2)^n$. The theory at each of these fixed points is similar: in a basis bringing the maximally relevant operator $\exp(im_j \phi_j)$ to $\exp(i\phi_1)$, ϕ_2 can be chosen so that the marginal operators at the fixed point are $\exp(i(\phi_1 \pm \phi_2)/2)$, and $\exp(i\phi_2)$ has scaling dimension 5 rather than 3 in the $\nu = 3/5$ case. The scaling dimension of the marginal operators is then $(\Delta(\phi_1) + \Delta(\phi_2))/4 = (1 + 5)/4 = 3/2$ as required. The marginal operators cannot form an $SU(3)$ multiplet with the maximally relevant operator because their scaling dimensions are different. We have not been able to obtain an exact solution of this fixed point. Appendix B describes the leading-order RG flows along the charge-unmixed line between points A and B and addresses the stability of the two types of fixed points. The reasons for the periodicity of Fig. 2 are discussed in Section IV.

Several $\dim K = 3$ non-principal edges of this type (antiparallel neutral modes) were studied, and all were found to have too few $|K(\mathbf{m})| = 2$ operators for the system to flow to a quantized σ . The four hierarchical states with K matrices $(1, 2, -4), (1, -2, 4), (1, -4, 2), (1, 4, -2)$, $\nu = (9/5, 9/13, 9/11, 9/7)$ are not T -stable and have only one $|K(\mathbf{m})| = 2$ operator. The two states with K matrices $(1, 4, -4)$ and $(1, -4, 4)$, $\nu = (17/13, 17/21)$ each have a Fibonacci sequence of $|K(\mathbf{m})| = 4$ operators as well as one $K(\mathbf{m}) = 2$ and one $K(\mathbf{m}) = -2$ operator. The resulting phase diagram for $\nu = 17/13$ is shown in Fig. 3. Most velocity matrices near the charge-unmixed line are not affected by either $|K(\mathbf{m})| = 2$ operator. If the starting V matrix makes the $K(\mathbf{m}) = -2$ operator relevant, the system is driven by impurity scattering to the $(0, 0)$ point on the charge-unmixed line. For starting points with this operator irrelevant, impurity scattering is insufficient to give edge equilibration at low temperatures.

Tuning the V matrix in the $\nu = 17/13$ state in principle allows a transition like the KFP transition for $\nu = 2/3$ to be observed, even if the system is always on the charge-unmixed line. Recall that for $\nu = 2/3$ the system has continuous, nonuniversal scaling dimensions as long as V is not too close to the charge-unmixed point. A Kosterlitz-Thouless type transition occurs when $|p| = \sqrt{5}/2$ in (3.2), and for $|p| \leq \sqrt{5}/2$ the system has a universal scaling dimension matrix. In the $\nu = 17/13$ state, as V is tuned on the charge-unmixed line the scaling dimension matrix is continuously variable until one of the disorder operators becomes relevant; then V is driven to one of the two fixed points, depending on which operator is relevant. Unfortunately the $\nu = 17/13$ state is expected to be quite difficult to observe, as it is a nonprincipal state with three condensates.

D. Edges with $\dim K = 4$

The edges with all neutral modes opposite the charge mode have a single charge-unmixed point in the three-dimensional space of boost parameters, while the other two types of edges (Table I) have a plane of charge-unmixed points. This section studies the charge-unmixed plane of four-condensate T -stable principal hierarchy states and finds a pattern with high symmetry and three different types of fixed points, two of which are exactly solvable. The states studied have $K = (l, 2, -2, 2)$ or $K = (l, -2, 2, -2)$, which were shown by Haldane to be the only $\dim K = 4$ T -stable principal hierarchy states with neutral modes traveling in both directions.¹² Examples are $\nu = 12/31$ with $K = (3, -2, 2, -2)$ and $\nu = 12/17$ with $K = (1, 2, -2, 2)$.

These states behave differently away from the charge-unmixed plane but have identical structures on the plane, where each state has two neutral modes traveling in one direction and one neutral mode traveling in the opposite direction as well as a decoupled charge mode. For definiteness we study the $\nu = 12/17$ state, although all four states $\nu = 12/7, 12/17, 12/31, 12/41$ have the same neutral sector. Each of these states has an infinite number of $|K(\mathbf{m})| = 2$ operators. For the $\nu = 12/17$ state, $K(\mathbf{m}) = 2$ operators are relevant on compact regions and $K(\mathbf{m}) = -2$ operators on noncompact regions of the plane. The maximally relevant points and contours are plotted in Fig. 4 as functions of boost parameters. The points and the intersections of the contours mark the position of fixed points. The points marked A, B, C are examples of the three different types of fixed points. Plotting the marginal contours of the $|K(\mathbf{m})| = 2$ operators gives Fig. 5a-c. Fig. 5a was obtained by choosing a basis to bring a point (A) of sixfold symmetry to the origin. There are also points of fourfold symmetry (B) as at the origin of Fig. 4, Fig. 5b, and Fig. 6, and points of twofold symmetry (C) as in Fig. 5c. There is no *a priori* reason to favor one type over the others. In the same way, Fig. 2 could have been drawn using a different basis to bring point B at the origin. The third type of fixed point has one operator maximally relevant and four marginal operators: these points are visible in Fig. 5a-c as the crossings of four marginal lines at the center of a marginal circle. These “double marginal” fixed points resemble the fixed points of the Fibonacci $\nu = 5/3$ state except that there are four rather than two marginal operators. Fig. 6 shows a curious property of these four-condensate edges: the most relevant contours plotted as functions of “velocity” coordinates rather than “momenta” p_i in (2.14) turn out to be straight lines. Marginal contours are not straight lines, even those which are straight lines in Fig. 5b. Mathematically the most relevant contours are straight because the square-root terms cancel in the equation $\Delta(\mathbf{m}) = 1$ which determines the contour, leaving only linear terms.

The complicated patterns in Fig. 5a-c have physical

consequences. The sixfold symmetric points like A have three maximally relevant operators and an $SU(3)$ symmetry identical to that of the $\nu = 3/5$ fixed point previously studied. The fourfold symmetric points like B have two independent $|K(\mathbf{m})| = 2$ operators and an $SU(2) \times SU(2)$ symmetry which is similar to the $SU(2)$ symmetry of the $\nu = 2/3$ fixed point. The double marginal points like C are shown in Section V to give a different tunneling exponent than the roughly similar $\nu = 5/3$ fixed point. These different phases within the charge-unmixed plane are important even if quantum Hall systems necessarily have quantized conductance, as has been suggested.¹² Points A and B are stable and solvable but are shown in Section V to have different measurable properties, so a single FQH edge with impurities can have several physically different stable phases.

A complete understanding of these $\dim K = 4$ states would require studying the three- or four-dimensional plots of which Fig. 5a-c are sections. One difference between the $\dim K = 4$ states and the states studied up to this point is that there are small regions of the charge-unmixed plane on which only one operator is relevant, making it less certain that points not on the plane but near one of these regions would flow toward the plane as required for robust quantization. The dashed line between A and B in Fig. 5a passes through one such region. Some experimental properties of the $\dim K = 4$ states are discussed in Section V.

IV. SYMMETRIES OF THE EDGE

This section discusses the effects of impurity scattering on the symmetries in the χ LL theories of various edges. The restoration of symmetry by impurity scattering will be shown to explain the patterns in the phase diagrams found in Section III. The χ LL theory of a quantum Hall edge contains two matrices K and V and a charge vector \mathbf{t} as described in Section II. The integer matrix K may admit discrete symmetries, which are described by integer matrices M invertible over the integers with

$$M^T K M = K, \quad M^T \mathbf{t} = \mathbf{t}. \quad (4.1)$$

Most velocity matrices V do not have such symmetries. Thus a symmetry possessed by K is in general broken by the V terms in the χ LL action.

One result of KFP is that impurity scattering can drive the velocity matrix to a fixed point where all the symmetries of K are symmetries of the full theory. In this section we show that, for the edges with infinitely many fixed points found in section III, impurity scattering sometimes restores some but not all of the symmetry of the K matrix. Because of this broken symmetry, the different fixed points are like spin-up and spin-down fixed points for an Ising ferromagnet below the transition temperature: the Ising fixed points are carried into each other by spin rotation, which is a symmetry of the starting Hamiltonian

but not of the fixed points. The infinitely many impurity fixed points are carried into each other by symmetries of K which are not symmetries of V at the fixed points. The broken-symmetry structure can be very rich, as in the case of the $\nu = 12/17$ state, which has three different types of fixed points, each breaking different symmetries of K .

The matrix M in (4.1) gives a transformation $\phi_i = M_{ij}\tilde{\phi}_j$ of the bosonic fields ϕ_i under which the action is form-invariant. The discrete symmetry transformation M can reflect an underlying continuous symmetry, as in the theory of the $\nu = 2/3, 3/5, 4/7, \dots$ states, where the discrete symmetries of the K matrix reflect an $SU(n)$ symmetry of the field theory, $n = \dim K$.¹⁹ It is easily seen that the symmetries M of a given K matrix form a group with matrix multiplication as the group product. The key difference between edges with a single impurity fixed point and edges with infinitely many fixed points is that the former have finite symmetry groups, while the latter have infinite symmetry groups. As examples of the two types, we find the symmetries of the $\nu = 3/5$ (finite) and $\nu = 5/3$ (infinite) edges. The results presented for $\nu = 5/3$ also apply to the other Fibonacci-type edges: $\nu = 5/7$, $\nu = 5/13$, $\nu = 5/17$. Section V shows that the two different types of fixed points in the $\nu = 5/3$ edge have different experimentally observable properties. The $\nu = 12/17$ edge (likewise $\nu = 12/7$, $\nu = 12/31$, $\nu = 12/41$) is shown to have three different types of fixed points related by a complicated symmetry group.

The $\nu = 3/5$ state in the hierarchy basis has

$$K = \begin{pmatrix} 1 & 1 & 0 \\ 1 & -2 & 1 \\ 0 & 1 & -2 \end{pmatrix}, \quad \mathbf{t} = (1, 0, 0). \quad (4.2)$$

One way to find the symmetries of K is to start with transformations W bringing K to diagonal form and preserving \mathbf{t} , as were used in Section III to obtain phase diagrams. Let D be the matrix with diagonal elements $(1, -1, 1)$. If $W^T K W$ is diagonal, then $M = W D W^{-1}$ is a symmetry of K with the property that $M^2 = I$, the identity. The effect of M is to use W to go to independent fields ϕ_i , change the sign of one field, and then return to the original fields. The problem is that M is only integral for some choices of W . One hopes that by choosing different matrices W_i , one can find enough integral M_i to generate the entire group of symmetries. The M_i are improper since $\det M_i = -1$; the proper symmetry group contains only products of even numbers of M_i .

For $\nu = 3/5$ two generators found using this trick are

$$x = \begin{pmatrix} 1 & 0 & 0 \\ 0 & 1 & 0 \\ 0 & 1 & -1 \end{pmatrix}, \quad y = \begin{pmatrix} 1 & 0 & 0 \\ 1 & -1 & 1 \\ 0 & 0 & 1 \end{pmatrix}. \quad (4.3)$$

The element xy is a proper symmetry which generates a 120° rotation of Fig. 1, and as expected $(xy)^3 = I$. The symmetry group has six elements: three proper elements

$\{I, xy, (xy)^2 = y^{-1}x^{-1}\}$ and three improper elements $\{x, y, xyx\}$. It is easy to check that these six elements are the full symmetry group G . The velocity matrix at the fixed point also has all of these symmetries. (For the sake of exactness, recall that the origin of Fig. 1 represents the set of all velocity matrices with certain values of the boost parameters, as described in Section II. There is an additional RG flow of the other parameters in V which makes the two neutral modes have the same velocity. Without this additional flow, only the boost part of the velocity matrix would have the symmetry.)

One simple consequence of the symmetry at the $\nu = 3/5$ fixed point is that the V -dependent scaling dimension matrix Δ , which determines the scaling dimension of the operator $O_{\mathbf{m}} = \exp(im_j \phi_j)$ according to $\Delta(\mathbf{m}) = m_i \Delta_{ij} m_j$, has the same symmetries as K^{-1} : $x \Delta x^T = y \Delta y^T = \Delta$. Note that Δ transforms like K^{-1} rather than K so its symmetries are transposed symmetries of K . At the fixed point Δ is invariant under all symmetries of K^{-1} for any edge with all neutral modes moving opposite the charge mode, as now shown. These edges have fixed points where K^{-1} and Δ are both diagonal in some integral basis with first basis vector $\mathbf{e}_1 = \mathbf{t}$. K^{-1} has all diagonal entries negative except for the first, and $2\Delta = |K^{-1}|$ has all diagonal entries positive. Any vector \mathbf{m} with charge $q = \mathbf{t} K^{-1} \mathbf{m}$ can be written as $\mathbf{m} = a\mathbf{t} + \mathbf{n}$, where \mathbf{n} has charge zero ($\mathbf{t} K^{-1} \mathbf{n} = 0$) and $a = \mathbf{t} K^{-1} \mathbf{m} / \mathbf{t} K^{-1} \mathbf{t} = q\nu^{-1}$. Now with $K(\mathbf{x}) = \mathbf{x} K^{-1} \mathbf{x}$,

$$2\Delta(\mathbf{m}) = 2\Delta(a\mathbf{t} + \mathbf{n}) = a^2 K(\mathbf{t}) - K(\mathbf{n}) = \frac{q^2}{\nu} - K(\mathbf{n}). \quad (4.4)$$

Let $\mathbf{m}' = M\mathbf{m}$ be the image of \mathbf{m} under a symmetry of K^{-1} . Then $2\Delta(\mathbf{m}') = q^2/\nu - K(\mathbf{n}') = q^2/\nu - K(\mathbf{n}) = 2\Delta(\mathbf{m})$, since $\mathbf{n}' = M\mathbf{n}$. Thus Δ has every symmetry of K^{-1} for any charge-unmixed fixed point in a state with all neutral modes opposite the charge mode. Broken-symmetry fixed points therefore appear only in states with neutral modes in both directions. The same argument gives that at any charge-unmixed fixed point where K and Δ are diagonal,

$$2\Delta(\mathbf{m}) \geq q^2/\nu \quad (4.5)$$

where q is the charge of \mathbf{m} . This inequality appears in the discussion of quasiparticles in Section V.

The same technique can be used to find the symmetries of K for the $\nu = 5/3$ Fibonacci-type edge shown in Fig. 2. Two elements of the symmetry group are found from changing the sign of $(1, -1, 0)$, which corresponds to reflecting $x \leftrightarrow -x$ in Fig. 2, and from changing the sign of $(0, 1, 3)$, which corresponds to reflecting the x -axis through the point B . The resulting matrices are

$$u = \begin{pmatrix} 0 & 1 & 0 \\ 1 & 0 & 0 \\ 0 & 0 & 1 \end{pmatrix}, \quad v = \begin{pmatrix} 1 & 0 & 0 \\ 0 & 2 & 3 \\ 0 & -1 & -2 \end{pmatrix}. \quad (4.6)$$

The difference between this case and the previous one appears when u and v are multiplied to obtain other group elements. The element $w \equiv uv$ is a proper symmetry of infinite order: I, w, w^2, \dots are all different matrices and all symmetries of K . Each application of w corresponds to translating Fig. 2 horizontally. The Fibonacci property $\mathbf{m}_{n+1} = \mathbf{m}_n + \mathbf{m}_{n-1}$ mentioned earlier is a consequence of symmetry under w . The powers of w and its inverse give the entire proper symmetry group, which is isomorphic to Z^+ , the group of integers under addition. The full symmetry group is isomorphic to the semidirect product of Z^+ and the binary group $\{1, -1\}$.

At each fixed point Δ has a much smaller symmetry group than K . The only symmetry of Δ at a fixed point other than I is the unique reflection which changes the sign of the operator maximally relevant at the fixed point. For example, u is a symmetry of point A ($u\Delta_A u^T = \Delta_A$) but v is not. It is apparent from Fig. 2 that some symmetry of K^{-1} is broken at each fixed point because neutral operators \mathbf{m}_i with the same minimum scaling dimensions $K(\mathbf{m}_i) = 2$ have different actual scaling dimensions $\Delta(\mathbf{m}_i)$. The matrix $w = uv$ is a symmetry of no fixed point, but its effect is to move the system from one fixed point to the next: $w\Delta_i w^T = \Delta_{i+1}$, where i labels fixed points of the same type, i.e., w never takes maximally relevant points of $K(\mathbf{m}) = -2$ operators to maximally relevant points of $K(\mathbf{m}) = 2$ operators, since w preserves K . Thus in Fig. 2 there is no symmetry taking point A to point B . In Section V it is shown that the two different types of fixed points have different experimentally measurable properties.

By applying symmetries of K , the boost part of any velocity matrix can be made to lie in the region bounded by the maximally relevant lines of $(1, -1, 0)$ and $(-1, 2, 3)$ in Fig. 2. This region is a “fundamental period” of the symmetries of K . However, different fixed points of the same type may correspond to experimentally different phases, even though they are related by a discrete symmetry and will have the same scaling dimensions, etc. The reason is that an experimental probe will couple nonuniversally to some combination of the original fields ϕ_i , which after applying a symmetry of K will be some different combination of the redefined fields ϕ'_i . Experiments will measure different prefactors for various quantities at different fixed points of the same type. Hence even if only points of type A are found to be stable for $\nu = 5/3$, for example, there would still be multiple edge phases with true transitions at phase boundaries. This is not true if there are *continuous* rather than discrete symmetries of the χ LL system relating fixed points of the same type, since then all the fixed points are continuously connected. Such a situation occurs if the discrete symmetries of the bosonized (K, V) theory arise from continuous symmetries of the underlying fermionic Lagrangian. We discuss this point further for the $\nu = 3/5$ state in Section VI. Stable fixed points of different types always give different phases.

Multiple-condensate edges have quite complicated

symmetry groups, and it is an interesting mathematical exercise to classify these groups in terms of familiar finitely generated groups. The symmetry group of $\nu = 3/5$ found above is D_3 , the triangular dihedral group, for example. Principal hierarchy states with all neutral modes opposite the charge mode have finite symmetry groups, and principal hierarchy states with neutral modes in both directions have infinite symmetry groups. Non-principal hierarchy states often have no nontrivial symmetries. Here we will be content to mention some results on the four-condensate principal hierarchy states discussed previously. The four-condensate states $\nu = 12/7, 12/17, 12/31, 12/41$ have three distinct types of fixed points (A, B, C in Fig. 5a-c). The phase diagram has six-fold symmetry about point A , fourfold symmetry about point B , and twofold symmetry about point C . It seems likely that these point symmetries are sufficient to generate the full symmetry group, which at point A is broken to a six-element subgroup and similarly for B and C . A fundamental period of the symmetry group is drawn in Fig. 5a. A set of generating matrices for $\nu = 12/17$ in the hierarchy basis is then

$$m_1 = \begin{pmatrix} 1 & 0 & 0 & 0 \\ 0 & 1 & 0 & 0 \\ 0 & 0 & 1 & 0 \\ 0 & 0 & 1 & -1 \end{pmatrix}, \quad m_2 = \begin{pmatrix} 1 & 0 & 0 & 0 \\ 1 & -1 & 1 & 0 \\ 0 & 0 & 1 & 0 \\ 0 & 0 & 0 & 1 \end{pmatrix},$$

$$m_3 = \begin{pmatrix} 1 & 0 & 0 & 0 \\ 0 & 1 & 0 & 0 \\ 0 & -1 & -1 & -1 \\ 0 & 0 & 0 & 1 \end{pmatrix}. \quad (4.7)$$

These m_i were obtained with the sign-flip procedure used above: for each i $\det m_i = -1$ and $m_i^2 = I$. The symmetries of point B are generated by m_1 and m_2 , which commute, and m_3 gives a rotation by π around point C . A sample element of order 3 is $m_1 m_3 m_2 m_3$, and an element of infinite order is $m_3 m_2$.

V. IMPLICATIONS FOR EXPERIMENT

The conductance and other experimental properties of a quantum Hall state are affected by disorder according to the RG flows described in the preceding sections. One important feature of the three- and four-condensate principal hierarchy states is that they can have multiple phases within the charge-unmixed subset of velocity matrices. This is different from the situation in two-condensate states and for any state with all neutral modes moving in the same direction, where the quantization of conductance occurs at a single point in boost-parameter space and no phase transitions are predicted within the charge-unmixed subset of velocity matrices.

In this section we first consider the $\nu = 5/3$ state and argue that experimental setups are likely to be close to point B in the phase diagram, Fig. 2. The $\nu = 5/7$

state probably offers the best chance for an experimentally accessible phase transition. We calculate electron and quasiparticle tunneling exponents for the different types of fixed points found in the preceding sections and show that different phases at the same filling fraction have different temperature dependences of electron tunneling through a barrier.

The $\nu = 5/3$ state seen experimentally is likely to contain both up spins and down spins: it consists of a $\nu = 1$ state of spin-up electrons and a $\nu = 2/3$ state of spin-down electrons, or vice versa. The fully polarized state has higher energy than the mixed-spin state because some electrons lie in the second Landau level rather than the first, costing energy proportional to $\hbar\omega_c$, ω_c the cyclotron frequency. This dominates the savings in the Zeeman and Coulomb energies from polarizing the spins, at least in GaAs, where the effective g -factor and Zeeman energy are small. The fully polarized state might appear in other materials with larger g , or in tilted-field configurations which allow the Zeeman energy to be increased with ω_c constant.

In the mixed-spin $\nu = 5/3$ state, scattering between up and down spins is expected to be very weak unless magnetic impurities are added. Thus the spin-up and spin-down components are largely independent. Independent $\nu = 1$ and $\nu = 2/3$ liquids are described by point B in Fig. 2 because the velocity matrix which has no interactions between the two liquids gives the scaling dimension matrix

$$2\Delta = \begin{pmatrix} 2\Delta_1 & 0 & 0 \\ 0 & 2\Delta_{2/3} & 0 \\ 0 & 0 & 2 \end{pmatrix} = \begin{pmatrix} 1 & 0 & 0 \\ 0 & 2/3 & 0 \\ 0 & 0 & 2 \end{pmatrix}, \quad \mathbf{t} = (1, 1, 0) \quad (5.1)$$

which is brought by a change of basis to point B . It is shown below that point B has the same low-temperature tunneling conductance exponent $G \sim T^0$ as a combination of a $\nu = 1$ state ($G \sim T^0$) and $\nu = 2/3$ state ($G \sim T^2$) would have. The fixed point A is not easily interpreted as a sum of two independent edges. At A the operator $(1, -1, 0)$ which hops charge between the two right-moving modes is maximally relevant, suggesting that in this phase the $\nu = 1/3$ left-moving mode pairs with a bound, $SU(2)$ symmetric combination of right-moving modes rather than with just one right-moving mode as at point B .

The $\nu = 5/7$ ground state is spin-polarized and its two edge fixed points may be more easily found experimentally than those of the $\nu = 5/3$ state. The $\nu = 5/7$ state is equivalent in K -matrix terms to a $\nu = 2/7$ gas of holes in a $\nu = 1$ state: $K_h = M^T K' M$, $M^T \mathbf{t}' = \mathbf{t}$, with $\mathbf{t}' = (1, 1, 0)$, $\mathbf{t} = (1, 0, 0)$,

$$K_h = \begin{pmatrix} 1 & 1 & 0 \\ 1 & -2 & 1 \\ 0 & 1 & 2 \end{pmatrix},$$

$$K' = \begin{pmatrix} K_1 & 0 & 0 \\ 0 & -K_{2/7} & 0 \\ 0 & 0 & 1 \end{pmatrix} = \begin{pmatrix} 1 & 0 & 0 \\ 0 & -3 & -1 \\ 0 & -1 & 2 \end{pmatrix}, \quad (5.2)$$

$$M = \begin{pmatrix} 1 & 1 & 0 \\ 0 & -1 & 0 \\ 0 & 0 & 1 \end{pmatrix}.$$

However, the V matrix $V_{1-2/7}$ with no interactions between the $\nu = 2/7$ holes and $\nu = 1$ electrons gives a conductance (in units of e^2/h) $\sigma = 9/7 = 1 + 2/7$ rather than $\sigma = 5/7 = 1 - 2/7$. This happens for exactly the same reason that a $\nu = 2/3$ state with velocity matrix describing $\nu = 1/3$ holes not interacting with $\nu = 1$ electrons gives a conductance $\sigma = 4/3$: the quantized value of conductance is only obtained if the edge equilibrates and all charged eigenmodes move in the same direction.

It is not difficult to find the point represented by $V_{1-2/7}$ in the $\nu = 5/7$ version of Fig. 2 (which looks similar but with some stretching along the y -axis): it lies on the y -axis with boost coordinates $(0, \sqrt{2/5})$. This is not a fixed point in the presence of disorder, and we expect the system to flow to a fixed point of type A or type B . Unlike in the $\nu = 5/3$ case, where type B was easily interpreted as a $\nu = 1$ state plus a $\nu = 2/3$ state with no interactions between the two, for $\nu = 5/7$ we have no simple interpretation of either phase as two independent subedges. The K matrix K_h is inequivalent to a combination of $\nu = 2/3$ and $\nu = 1/21$ because $\det K_h \neq (\det K_{2/3})(\det K_{1/21})$, so no invertible integral basis change can relate the two. Below we show that the A and B phases can be distinguished experimentally, so that measurements of a $\nu = 5/7$ sample edge would allow its phase to be determined. Then changes in the V matrix (from changes in the gate voltages, e.g.) might drive a new type of impurity phase transition.

Before calculating tunneling properties for the various fixed points, we would like to suggest briefly an experimental approach to edge impurity scattering based on the existence of spin-polarized and spin-singlet states at $\nu = 2/3$. At $\nu = 2/3$ there is an unpolarized spin-singlet state with the same K matrix and charge vector as the well-known spin-polarized state. The polarized state is naturally interpreted as the particle-hole conjugate of the Laughlin $\nu = 1/3$ state², while the unpolarized state is *not* the double-layer state consisting of a spin-up $\nu = 1/3$ state and a spin-down $\nu = 1/3$ state, which has an inequivalent K matrix. The unpolarized state can be studied in tilted-spin experiments such as those of Eisenstein *et al.*²⁶ and appears because of the relatively low Zeeman energy in GaAs as suggested by Halperin.²⁷ The KFP treatment should be just as valid for the unpolarized edge as for the polarized edge because they have the same K matrix. The unpolarized edge has an exact $SU(2)$ symmetry if the Zeeman energy is ignored, however, and this symmetry has physical consequences.

Numerical results on the unpolarized edge show that at low energy there are two branches of excitations, one spin-singlet charge branch and one spin branch described

by the $SU(2)$ Kac-Moody algebra.²⁸ This is the structure found at the KFP fixed point and different from the numerical results on the clean polarized edge, which indicate two spatially separated subedges with no special symmetry.^{29,30} It seems logical that the physical requirement of $SU(2)$ spin symmetry of the unpolarized edge forces the system to the KFP fixed point even in the absence of disorder, assuming the “hidden” $SU(2)$ symmetry is only found at the fixed point. The $SU(2)$ structure of the unpolarized edge is found in a small system (hence without RG flows) for both Coulomb and short-range interactions. The separation of the $\nu = 2/3$ edge into charge modes and neutral modes can thus be caused by (i) an exactly charge-unmixed velocity matrix, (ii) an unbroken $SU(2)$ symmetry, or (iii) random impurities. The possibility that impurities affect the polarized edge but not the unpolarized edge suggests that measurements of the edge equilibration length and tunneling conductance across the topological phase transition³¹ between the two may be illuminating.

In FQH states the tunneling conductance through a point constriction in a Hall bar decreases with decreasing temperature. In the integer effect this conductance is temperature-independent. The physical electron operator is a superposition of all charge- e fermionic operators, and the low-temperature conductance is determined by the scaling dimension Δ_e of the most relevant such operator according to^{32,33}

$$G(T) \approx t^2 T^{2(2\Delta_e - 1)} \quad (5.3)$$

where t is the amplitude for the dominant tunneling process. Different fixed points in the same FQH state can have different Δ_e and different tunneling exponents. These exponents can be calculated for the marginal-type fixed points even though the electron dynamics at these points is unclear. All fixed points of the same type have the same scaling exponents but are expected to have measurably different prefactors as described in Section IV.

Charge- e operators \mathbf{m} have $t_i K_{ij}^{-1} m_j = 1$ and scaling dimension $\Delta_e = m_i \Delta_{ij} m_j$ where Δ is the same symmetric matrix calculated in Section III. Since Δ is known at each fixed point, it is simple to search for the most relevant charge- e operator. The $SU(n)$ fixed points found by Kane and Fisher for the $\nu = n/(2n - 1)$ states have $2\Delta_e = 3 - 2n^{-1}$ and tunneling exponent

$$G(T) \approx t^2 T^\alpha, \quad \alpha = 4 - 4n^{-1}. \quad (5.4)$$

In Table II we list the low-temperature conductance behavior for each of the fixed points found in Section III. Note that corresponding fixed points in states with the same neutral sector, such as $\nu = 5/3$ and $\nu = 5/7$, can have different tunneling exponents because the charge sectors of the two edge theories are different. The Fibonacci-type states have two possible values of the low-temperature tunneling conductance exponent, so that there is a real physical difference between the A and B phases.

The level four states studied ($\nu = 12/7, 12/17, 12/31, 12/41$) have three different tunneling exponents corresponding to the three different types of fixed points. For example, in the $\nu = 12/17$ state the $SU(3)$ fixed points have $\Delta_e = 7/6$ and $\alpha = 8/3$ as appear in the $SU(3)$ fixed point of the $\nu = 3/5$ state. The $SU(2) \times SU(2)$ fixed point is the same as the $SU(2)$ fixed point for $\nu = 2/3$ except that there are two charge- e operators of minimal scaling dimension rather than one. The double marginal fixed point has an operator with $\Delta_e = 11/12$ so $\alpha = 5/3$. So the three different fixed points have three different values of α : $5/3$ for the double marginal points, 2 for the $SU(2) \times SU(2)$ points, and $8/3$ for the $SU(3)$ fixed points.

Other tunneling experiments are sensitive to the most relevant quasiparticle operator at a fixed point, rather than the most relevant electron operator. One experiment sensitive to the quasiparticle scaling dimension is tunneling through a slight constriction rather than through a deep constriction as described above.²⁰ We have calculated the scaling dimension of the most relevant quasiparticle operators for the various fixed points. No simple patterns are observed: often two or more quasiparticle operators have nearly the same minimum scaling dimension, and the charge of the most relevant quasiparticle operator varies among different fixed points of the same edge. As an example, in the $12/17$ edge the most relevant quasiparticles at the different fixed points are: $2\Delta = 5/17$, $q = 3e/17$ at the $SU(3)$ points, $2\Delta = 6/17$, $q = 2e/17$ at the $SU(2)$ points, and $2\Delta = 43/102$, $q = e/17$ at the double-marginal points. Typically the most relevant quasiparticles have small charges, as expected from the inequality (4.5).

Time-domain experiments have so far not resolved the neutral modes in nonchiral edge states,⁵ but in principle a perturbation at one contact on a sample edge should excite propagating charged and neutral modes observable at another contact. Such an experiment might reveal whether the neutral modes in the Fibonacci-type states $\nu = 5/3, 5/7, 5/13, 5/17$ propagate or are localized. The measurement of edge equilibration lengths might also give interesting results: measurements on the edge of the $\nu = 4/5$ edge, which has no $|K(\mathbf{m})| = 2$ operators and hence no KFP-type instability, could show another type of equilibration mechanism (such as inelastic scattering from phonons) with a different temperature dependence.

VI. SUMMARY

We have developed a technique for studying impurity scattering in a general FQH edge and used it to find phase diagrams and experimentally measurable properties for a broad class of nonchiral edges. We find that some FQH edges can have several different phases (fixed points) in the presence of randomness. These phases in general have higher symmetry at low energies and long wavelengths

than the original system. Thus random edges demonstrate an interesting phenomenon of dynamical restoration of symmetries at low energies and long length scales. Different phases have different experimentally observable properties. It would be very interesting to find these phases and study transitions between them experimentally.

The transitions between phases are interesting from the point of view of Landau's symmetry breaking principle for continuous transitions: A continuous phase transition (second-order in the Ehrenfest classification) can only occur between two phases which differ in symmetry, and the symmetries of one phase are a subset of the symmetries of the other phase. This principle appears to be satisfied by all the transitions between definitely stable fixed points in the edges we study. The principle is satisfied even though the RG flows for some transitions (such as the $\nu = 2/3$ transition¹¹) are similar to those in the Kosterlitz-Thouless transition, which is not clearly interpreted in terms of a broken symmetry. The symmetry breaking principle also has some implications for a possible phase transition in the $\nu = 5/3$ state, which has two types of possibly stable fixed points.

To summarize our results, two situations, with or without long-range interactions, need to be discussed separately. In the absence of long-range interactions, all the edge modes, in general, carry some amount of charge and the edge is called charge-mixed. Several different situations are illustrated by the following examples.

- The $\nu = 2/3$ edge has two phases. In one phase the edge is charge-mixed and the two-terminal conductance σ and the exponent α of electron tunneling between two edges $\sigma_{tun} \propto T^\alpha$ are not universal. In the other phase the edge has an $SU(2)$ symmetry and is charge-unmixed (*i.e.* only one propagating mode, the charge mode, carries charge and other propagating modes are neutral). In this case (σ, α) take universal values $(\frac{2}{3} \frac{e^2}{h}, 2)$.
- The $\nu = 3/5$ edge has three phases, described by a fixed point (the point (0, 0) in Fig. 1), fixed lines (the solid lines outside the hexagon bounded by the dashed lines in Fig. 1) and fixed planes (the region outside the region bounded by the dashed lines). This is because a point on the fixed planes does not flow as the energy is lowered, while a point between two parallel dashed lines flows to the fixed line between them and a point inside the hexagon flows to the fixed point. The fixed point has an $SU(3)$ symmetry and is charge-unmixed. $(\sigma, \alpha) = (\frac{3}{5} \frac{e^2}{h}, \frac{8}{3})$ are universal. The fixed-line and fixed-plane phases are charge-mixed and (σ, α) are not universal. But in the fixed-line phase there is an $SU(2)$ symmetry and (σ, α) and other exponents all depend on a single parameter which parametrizes the fixed line. The fixed-plane phase has no particular symmetries. We would like to point out that although the

fixed-line phase in Fig. 1 contains six disconnected segments, this does not guarantee that there are six disconnected fixed-line phases. This is because the disconnected fixed lines may be connected in a higher-dimensional space of Lagrangians of which Fig. 1 is just a two-dimensional cross section. If different line segments are connected in the enlarged space, it is possible to move continuously from one segment to another without any transition. For the $\nu = 3/5$ state the higher-dimensional space results from applying the $SU(3)$ transformation on the full Lagrangian. Note that the $SU(3)$ transformation does not change the commutators between fermions (which can be seen in the fermionic form of the Lagrangian but is not evident in the (Abelian) bosonized form), and hence leaves the Hilbert space unchanged. Acting with the $SU(3)$ generators creates off-diagonal interaction terms of the form $f(x)(\bar{\psi}_1\psi_2)(\bar{\psi}_2\psi_1)$, after we make the local $SU(3)$ transformation to remove the random hopping term between different fermions. Thus the precise form of the function $f(x)$ depends on the impurities which generate the random hopping terms. If the off-diagonal terms have precisely the variable coefficients $f(x)$, then the different fixed-line phases can be continuously connected via inclusion of such off-diagonal terms. However, in real experiments it is impossible to control the precise form of the variable coefficients $f(x)$, and the Lagrangians for experimental samples do not contain the above off-diagonal terms. Therefore for real samples all different fixed-line phases are disconnected. Similarly all fixed planes are disconnected for real samples. However, since fixed-line phases (or fixed-plane phases) all have the same symmetry, the symmetry breaking principle prohibits continuous phase transitions between two connected fixed-line phases or two connected fixed-plane phases. But there are still continuous phase transitions between a fixed-line phase and a fixed-plane phase, and a fixed-line phase and a fixed-point phase.

We would like to stress that the sequence of the phase transition: fixed-point phase \rightarrow fixed-line phase \rightarrow fixed-plane phase represents a sequence of symmetry breaking: $SU(3) \rightarrow SU(2) \rightarrow SU(1)$. This is consistent with the symmetry breaking principle discussed above. It appears that the symmetry breaking principle that governs the continuous transitions between clean phases in other condensed matter systems also governs the continuous transitions between disordered phases of FQH edges. All the continuous phase transitions between different disordered edge phases that we find in this paper are related to symmetry breaking.

- The $\nu = 5/3$ edge also has three (types of) phases described by fixed points (such as B in Fig. 2, but not A), fixed lines (the solid lines in Fig. 2) and

fixed planes (the region outside the region bounded by the dashed lines). Again the fixed-point phase is charge-unmixed and has universal (σ, α) . The fixed-line and fixed-plane phases are charge-mixed and have non-universal (σ, α) . However, here the fixed point contains two marginal operators. It is not clear whether the fixed point is stable or not (depending on whether the two marginal operators are marginally relevant or not). It is not clear if different fixed lines and fixed planes are connected or not in a higher-dimensional space. There is a continuous phase transition between the fixed-line phase (with $SU(2)$ symmetry) and fixed-plane phase (with no symmetry). We note that both the fixed-point phase and the fixed-line phase have $SU(2)$ symmetry. According to the symmetry breaking principle for continuous transition, either there is another phase separating the fixed-point phase and the fixed-line phase, or the fixed-point phase is unstable, or the transition is first-order (discontinuous) and the first-order line does not terminate in a second-order point for any finite disorder strength. The perturbative RG in Appendix B is consistent with the last possibility.

- The $\nu = 17/13$ edge ($K = (1, 4, -4)$) again has three phases described by a fixed point, a fixed line and a fixed plane. (Fig. 3) However, the phase diagram is quite different from the above two. There can only be continuous phase transitions between the following phases: the fixed-point phase (with $SU(2)$ symmetry) \longleftrightarrow the fixed-plane phase (with no symmetry) \longleftrightarrow the fixed-line phase (with $SU(2)$ symmetry).
- The $K = (l, 2, -2, 2)$ and $K = (l, -2, 2, -2)$ edges are too complicated, and we will only discuss them for the case of long-range interactions.

In the presence of long-range interactions the edge is always (nearly) charge-unmixed and the two-terminal conductance always takes the quantized value $\sigma = \nu \frac{e^2}{h}$. We can restrict our discussion to the charge-unmixed subspace (the $(0, 0)$ point in Fig. 1 and the x -axis in Fig. 2 and 3). Table II gives the low-temperature tunneling exponent for all the charge-unmixed phases of principal hierarchy states. The above examples with short-range interactions can be easily modified to cover the case of long-range interactions:

- The $\nu = 2/3$ edge has only one phase which is described by a fixed point. (σ, α) take universal values $(\frac{2}{3} \frac{e^2}{h}, 2)$.
- The $\nu = 3/5$ edge has only one phase, described by a fixed point (the point $(0, 0)$ in Fig. 1). The fixed-point phase is the same as the fixed-point phase for short-range interactions: it has an $SU(3)$ symmetry and universal $(\sigma, \alpha) = (\frac{3}{5} \frac{e^2}{h}, \frac{8}{3})$.

- The $\nu = 5/3$ edge has two (types of) phases described by A -type and B -type fixed points in Fig. 2. The fixed-point phases have universal α given by $\alpha = 2/5$ for A -type and $\alpha = 0$ for B -type. However both A -type and B -type fixed points contain two marginal operators, and it is not clear whether the fixed points are stable.
- The $\nu = 17/13$ edge ($K = (1, 4, -4)$) has three phases described by two fixed points (A and B in Fig. 3) and a fixed line (the x -axis outside the region bounded by the dashed lines). All three phases are stable. The two fixed-point phases have different universal values for the temperature exponent: $\alpha = 2$ for the A -type and $\alpha = 18/17$ for the B -type fixed-point phase. α is not universal for the fixed-line phase. The only continuous phase transitions are between one of the two fixed-point phases ($SU(2)$ symmetry) and the fixed-line phase (no symmetry).
- The $K = (l, 2, -2, 2)$ and $K = (l, -2, 2, -2)$ edges with $\nu = 12/7, 12/17, \dots$ are very interesting. There are four different phases described by three types of fixed points (A, B, C in Fig. 4 and 5) and a fixed line (the middle segment of the dashed line connecting A and B in Fig. 5a). Certainly there are infinitely many different disconnected A -, B -, C -type fixed points and fixed lines in Fig. 5a, and it is not clear if all fixed points (lines) of each type are connected in a higher-dimensional space. The A -type fixed point has an $SU(3)$ symmetry, the B -type fixed point has an $SU(2) \times SU(2)$ symmetry, the fixed line and the C -type fixed point have an $SU(2)$ symmetry. The exponent α has the universal values $(8/3, 2, 5/3)$ for the A -, B -, C -type fixed points respectively. The C -type fixed point has four marginal operators and it is not clear whether it is a stable fixed point. Among the three definitely stable phases the only possible continuous transitions are: A -type phases ($SU(3)$ symmetry) \longleftrightarrow fixed-line phase ($SU(2)$ symmetry) \longleftrightarrow B -type phases ($SU(2) \times SU(2)$ symmetry). These transitions are consistent with the symmetry breaking principle for continuous transitions. An A -type \longleftrightarrow B -type transition would violate the symmetry breaking principle and is not found in the phase diagram.

This study just starts to reveal some general intrinsic structures of disordered phases of FQH edges and transitions between those phases. It is amazing to see that different disordered phases are characterized by symmetries and that phase transitions are characterized by broken symmetries. Certainly there are many open problems and much needs to be done in order to have a complete theory of disordered edges. The possibilities of transitions between different disordered phases on the edge of

a single bulk quantum Hall liquid also open up new directions for experimental explorations.

J. E. M. wishes to thank W. R. Mann and C. Mudry for helpful conversations. X.-G. W. is supported by NSF Grant No. DMR-97-14198 and NSF-MRSEC Grant No. DMR-94-00334. J. E. M. acknowledges a fellowship from the Fannie and John Hertz Foundation.

APPENDIX A: BOOSTS AND ROTATIONS

The decomposition of an element of $SO(m, n)$ into a product of a boost and a rotation follows in a neighborhood of the origin simply by writing the product $M = BR$ in terms of infinitesimal generators of the Lie group. If b_i are the boost generators and r_i the rotation generators, then a boost (similarly, rotation) close to the identity element contains only boost (rotation) generators:

$$BR = (1 + \epsilon_i b^i)(1 + \delta_j r^j) \approx 1 + \epsilon_i b^i + \delta_j r^j, \quad (\text{A1})$$

where ϵ_i and δ_j are arbitrary infinitesimal parameters. There are exactly enough free parameters to cover a neighborhood of the identity in $SO(m, n)$. Thus if the decomposition does not hold on the entire group, there must be some boundary in $SO(m, n)$ where it ceases to hold. In the next paragraph we outline a global proof of the decomposition. The details are given for $SO(m, 1)$, which is the only case used in the body of this paper.

The boost part of a given matrix M can be constructed if every symmetric positive definite element of $SO(m, n)$ has a square root within the group which is also symmetric. The square root is simple for $m = 1$ or $n = 1$, where every symmetric positive definite matrix is of the form introduced in Section II and associated with a unique velocity vector $\mathbf{v} = \mathbf{p}/\gamma$. Then the square root is the boost with velocity $\mathbf{v}' = \mathbf{v}(1 - \sqrt{1 - v^2})/v^2$, which is chosen so that the special-relativistic velocity addition formula holds: $\mathbf{v} = 2\mathbf{v}'/(1 + v'^2)$. For the general $SO(m, n)$ case, a square root can be defined by the Inverse Function Theorem within a neighborhood of the identity and analytically continued. Such a square root exists globally if every boost matrix can be written as an exponential of only boost generators, since then

$$B' = \exp \begin{pmatrix} \mathbf{0} & b \\ b^T & \mathbf{0} \end{pmatrix}, \quad \sqrt{B'} = \exp \begin{pmatrix} \mathbf{0} & \frac{b}{2} \\ \frac{b^T}{2} & \mathbf{0} \end{pmatrix}. \quad (\text{A2})$$

With a square root, the proof is simple. Given an arbitrary element $M \in SO(m, n)$, MM^T is symmetric and positive definite, so let $B \equiv \sqrt{MM^T}$. It remains to show that $R \equiv B^{-1}M$ is in $SO(m, n)$ and is orthogonal:

$$\begin{aligned} RI_{m,n}R^T &= B^{-1}MI_{m,n}M^TB^{-1T} \\ &= B^{-1}I_{m,n}B^{-1T} = I_{m,n}, \end{aligned} \quad (\text{A3})$$

$$\begin{aligned} R^TR &= (\sqrt{MM^T}^{-1}M)^T(\sqrt{MM^T}^{-1}M) \\ &= M^T(\sqrt{MM^T}^2)^{-1}M = I. \end{aligned} \quad (\text{A4})$$

APPENDIX B: RENORMALIZATION GROUP TREATMENT OF THE FIBONACCI EDGE

The exactly solvable $SU(2)$ fixed point found by KFP is stable under RG transformations: near the fixed point the velocity matrix weakly couples the modes which are decoupled at the fixed point, but this originally marginal term in the action acquires a random coefficient from the $SU(2)$ rotation and becomes irrelevant. The fixed point is no longer necessarily stable if there is an additional marginal disorder operator, since this term has a random coefficient to begin with and does not have its scaling dimension decreased by the $SU(2)$ rotation. Therefore such a term remains marginal and must be treated. In this section we obtain the first-order coupled RG equations for the Fibonacci-type edge $\nu = 5/3$, which has additional marginal operators present at each of its fixed points.

These first-order equations suggest that both types A and B of fixed points are in fact stable and that which fixed point the system flows to asymptotically depends on the initial velocity matrix and the disorder strengths. The picture from the first-order equations is incomplete at the fixed point because the higher-order effects of one disordered operator upon another are ignored, although these effects may well determine the properties of the fixed point. The main conclusion of the somewhat complicated discussion below is that the fixed points with marginal operators are probably stable under RG transformations although the long-length-scale dynamics at the fixed point are unclear. Note that even if only one type of fixed point turns out to be stable, different fixed points of that type are distinguishable phases as discussed in Section IV. Fixed points of the same type have the same stability properties because they have the same χLL theory up to a redefinition of fields.

For the calculation on the $\nu = 5/3$ edge, we will assume that the system is on the charge-unmixed line and use the scaling dimension of one operator Δ_1 as a coordinate on this line. This is reasonable since points close to the line are driven to the line under RG by the $K(\mathbf{m}) = -2$ operators. It is possible that the strengths of all $K(\mathbf{m}) = -2$ operators may decrease sufficiently rapidly that the system is left on one of the $K(\mathbf{m}) = 2$ marginal lines away from the charge-mixed point. Then there is only one relevant operator and the fixed point is solvable with an $SU(2)$ symmetry, exactly as for the $\nu = 2/3$ fixed point studied by KFP. Only on the charge-unmixed line does a new type of fixed point appear.

At most three disorder operators can be relevant at a point on the charge-mixed line. One operator's scaling dimension serves as an independent coordinate and

determines the other scaling dimensions: writing Δ_1 for the scaling dimension of the operator whose maximally relevant point will be studied, the scaling dimensions of the two neighboring operators (Fig. 2) are the two roots Δ_{\pm} of

$$\Delta_{\pm}^2 - 3\Delta_{\pm}\Delta_1 + \Delta_1^2 + \frac{5}{4} = 0. \quad (\text{B1})$$

The disorder strength of each operator has leading-order RG flow $dD_i/d\ell = (3 - 2\Delta_i)D_i$. It remains to calculate how the velocity matrix and scaling dimensions flow.

The decomposition of the velocity matrix in Section III into a boost part which determines the scaling dimensions, plus a remaining “rotational” part, is *not* compatible with the RG transformation. The rotational part affects the flow of the boost part and vice versa. However, the qualitative character of the boost part is in some sense not affected by the rotational part as now explained. (Note that the K matrix is invariant under the RG transformation because it is purely topological and does not enter the Hamiltonian.) Consider the perturbative RG flow equation for the scaling dimension of the one $|K(\mathbf{m})| = 2$ operator for the $\nu = 2/3$ edge:¹¹

$$\frac{d\Delta}{d\ell} = -8\pi \frac{\sqrt{v_+ v_-^{-3}}}{v_+ + v_-} (\Delta^2 - 1)D. \quad (\text{B2})$$

The eigenmode velocities v_+ , v_- are in the rotational part of the velocity matrix and flow according to

$$\frac{dv_{\pm}}{d\ell} = -4\pi \frac{v_{\pm}^2}{\sqrt{v_+ v_-^5}} (\Delta \mp 1)D. \quad (\text{B3})$$

The eigenmode velocities affect how fast Δ flows to 1, but the basic idea that Δ flows smoothly to 1 is independent of the precise values of v_+ and v_- and of the details of their flow. In order to make the coupled RG flows tractable we will replace velocity-dependent prefactors by constants.

Suppose that the system is in between the maximally relevant points of two disorder operators with strengths D_1, D_2 . Then from (B1) the scaling dimensions flow as

$$\begin{aligned} \frac{d\Delta_1}{d\ell} &= -c_1(\Delta_1^2 - 1)D_1 \\ &\quad + c_2 \frac{3\Delta_1 - 2\Delta_2}{3\Delta_2 - 2\Delta_1} (\Delta_2^2 - 1)D_2, \end{aligned} \quad (\text{B4})$$

$$\begin{aligned} \frac{d\Delta_2}{d\ell} &= -c_2(\Delta_2^2 - 1)D_2 \\ &\quad + c_1 \frac{3\Delta_2 - 2\Delta_1}{3\Delta_1 - 2\Delta_2} (\Delta_1^2 - 1)D_1, \end{aligned} \quad (\text{B5})$$

with c_1 and c_2 some positive constants. These two equations are not independent and each together with (B1) determines the other. A complete set of first-order equations consists of one scaling-dimension equation plus the

flow of the disorder strengths, with the other scaling dimension found by (B1). The two disorder operators compete to drive the system to one of the maximally relevant points. The disorder strength flow implies that the fixed point which must exist somewhere between the two maximally relevant points is unstable, as expected, because on each side of this unstable point the disorder strength pushing the system away is the more rapidly growing of the two disorder operators. What happens at one of the maximally relevant points is a little tricky, because at such a point one disorder strength D_1 is growing rapidly but does not push the system in either direction since $\Delta^2 - 1 = 0$.

The main physical question to be settled is whether the disorder strength of one of the marginal operators becomes infinite, remains finite, or decreases to zero as the system moves to the fixed point. Now we show that in the leading-order equations the marginal disorder strengths remain finite as the system decays exponentially to the fixed point. This does not necessarily mean that the disorder strength of a marginal operator actually remains finite, since exactly at the fixed point this disorder strength is a constant to leading order but may increase or decrease at higher order. Linearizing the flow equations about $\Delta_1 = 1, \Delta_2 = 3/2$, and keeping Δ_2 as independent variable and writing $\epsilon = 3/2 - \Delta_2 > 0$, we have

$$\frac{dD_1}{d\ell} = (1 - 4\epsilon^2/5)D_1 \approx D_1, \quad (\text{B6})$$

$$\frac{dD_2}{d\ell} = 2\epsilon D_2, \quad (\text{B7})$$

$$\begin{aligned} \frac{d\epsilon}{d\ell} &= -c_2(9/4 + 3\epsilon - 1)D_2 + c_1\epsilon D_1 \\ &\approx -5c_2 D_2/4 + c_1\epsilon D_1. \end{aligned} \quad (\text{B8})$$

An asymptotic solution is found by taking $D_1 = D_1(0) \exp(\ell), \epsilon = A \exp(-\ell)$. The right side of (B8) will balance if $D_2 \rightarrow 4c_1 A/5c_2$ as $\ell \rightarrow \infty$ since the left side is much smaller in magnitude. This limiting form is consistent since with this form of ϵ , (B7) yields a finite $D_2 = \exp(\int 2\epsilon d\ell)$. The linearized analysis suggests that eventually the system decays exponentially to the fixed point with D_2 asymptotically finite. This prediction is confirmed by numerical integration of the original differential equations. Which fixed point the system reaches as $\ell \rightarrow \infty$ depends the initial scaling dimensions and disorder strengths.

A more complete RG treatment would give a deeper understanding of the fixed points, but determining the RG equations to second order in the disorder becomes quite complicated. We discuss some features here and hope to treat this problem more fully in another publication. A preliminary step is to assume that the system is driven near the fixed point by the first-order terms in the equation and then to carry out an $SU(2)$ rotation to eliminate the random term with the maximally relevant operator. If the impurity operators are uncorrelated, the marginal operators will still have random

coefficients. However, it is physically likely that different impurity operators will be at least partially correlated, possibly giving a uniform coefficient for the marginal operator, which then becomes relevant. In the case of uncorrelated impurities, the possibility of carrying out this rotation shows that no terms involving D_1 appear in the flow equation for D_2 exactly at the fixed point, so there is still hope for a perturbative treatment. Near but not at the fixed point, the $SU(2)$ rotation of the dominant impurity operator may affect the marginal operator even if the impurities are uncorrelated. Even if the second-order terms in this case have the proper sign to drive D_2 to zero, $dD_2/d\ell \propto -D_2^2$, the decrease of D_2 is only as $1/\ell$ rather than $\exp(-\ell)$, and at finite temperature the marginal operators should have significant effects. Another approach to understanding the marginal fixed point is via an exact solution, which we have not been able to find.

-
- ¹ K. von Klitzing, G. Dorda, and M. Pepper, Phys. Rev. Lett. **45**, 494 (1980).
- ² R. B. Laughlin, Phys. Rev. Lett. **50**, 1395 (1983).
- ³ B. I. Halperin, Phys. Rev. B **25**, 2185 (1982).
- ⁴ F. Milliken, C. Umbach and R. Webb, Solid State Comm., **97**, 309 (1995); A.M. Chang, L.N. Pfeiffer and K.W. West, Phys. Rev. Lett., **77**, 2538 (1996).
- ⁵ R. C. Ashoori, H. Stormer, L. Pfeiffer, K. Baldwin and K. West, Phys. Rev. B **45**, 3894 (1992).
- ⁶ For a review, X.-G. Wen, Adv. in Phys. **44**, 405 (1995).
- ⁷ S. M. Girvin and A. H. MacDonald, Phys. Rev. Lett. **58**, 1252 (1987); S. C. Zhang, T. H. Hansson and S. Kivelson, Phys. Rev. Lett. **62**, 82 (1989); N. Read, Phys. Rev. Lett. **62**, 86 (1989); Phys. Rev. Lett. **65**, 1502 (1990); X.-G. Wen and A. Zee, Nucl. Phys. **B15**, 135 (1990); B. Blok and X.-G. Wen, Phys. Rev. **B42**, 8133 (1990); Phys. Rev. **B42**, 8145 (1990); J. Fröhlich and A. Zee, Nucl. Phys. **B364**, 517 (1991).
- ⁸ X.-G. Wen, Phys. Rev. B **43**, 11025 (1991); Phys. Rev. Lett. **64**, 2206 (1990).
- ⁹ F. D. M. Haldane, Phys. Rev. Lett. **47**, 1840 (1981); J. M. Luttinger, J. Math. Phys. **4**, 1154 (1963); S. Tomonaga, Prog. Theor. Phys. **5**, 544 (1950).
- ¹⁰ C. W. J. Beenakker and H. van Houten, in *Solid State Physics*, eds. H. Ehrenreich and D. Turnbull (Academic, New York, 1991), vol. 44.
- ¹¹ C. L. Kane, M. P. A. Fisher, and J. Polchinski, Phys. Rev. Lett. **72**, 4129 (1994).
- ¹² F. D. M. Haldane, Phys. Rev. Lett. **74**, 2090 (1995).
- ¹³ C. L. Kane and M. P. A. Fisher, Phys. Rev. B **52**, 17393 (1995).
- ¹⁴ M. Büttiker, Phys. Rev. B **38**, 9375 (1988).
- ¹⁵ B. W. Alphenaar, P. L. McEuen, R. G. Wheeler, and R. N. Sacks, Phys. Rev. Lett. **64**, 677 (1990).
- ¹⁶ L. P. Kouwenhoven *et al.*, Phys. Rev. Lett. **64**, 685 (1990).
- ¹⁷ Y. Takagaki *et al.*, Phys. Rev. B **50**, 4456 (1994).
- ¹⁸ KFP argue that long-range Coulomb interactions included in the low-energy field theory give corrections of order $\log^{-2}(L/\ell)$ to the conductance, with L the screening length and ℓ the magnetic length, and that such corrections are not observed experimentally. Another model is that described in the text: contact interactions but with the charge-charge term larger than the charge-neutral term after integrating the interaction up to the screening length. In any event it seems quite plausible that current experimental setups are almost charge-unmixed.
- ¹⁹ N. Read, Phys. Rev. Lett. **65**, 1502 (1990).
- ²⁰ C. L. Kane and M. P. A. Fisher, Phys. Rev. B **51**, 13449 (1994).
- ²¹ F. D. M. Haldane, Phys. Rev. Lett. **51**, 605 (1983).
- ²² B. I. Halperin, Phys. Rev. Lett. **52**, 1583 (1984).
- ²³ G. L. Watson, *Integral Quadratic Forms* (Cambridge University Press, Cambridge, 1960), chaps. 1-3.
- ²⁴ T. Giamarchi and H. J. Schultz, Phys. Rev. B **37**, 325 (1988).
- ²⁵ C. W. Misner, K. S. Thorne and J. A. Wheeler, *Gravitation* (W. H. Freeman and Co., New York, 1973), p. 69.
- ²⁶ J. P. Eisenstein, H. L. Stormer, L. N. Pfeiffer, and K. W. West, Phys. Rev. Lett. **62**, 1540 (1989); Phys. Rev. B **41**, 7910 (1990).
- ²⁷ B. I. Halperin, Helv. Phys. Acta. **56**, 75 (1983).
- ²⁸ J. E. Moore and F. D. M. Haldane, Phys. Rev. B **55**, 7818 (1997).
- ²⁹ M. D. Johnson and A. H. MacDonald, Phys. Rev. Lett. **67**, 2060 (1991).
- ³⁰ X.-G. Wen, Int. J. Mod. Phys. B **6**, 1711 (1992).
- ³¹ I. A. McDonald and F. D. M. Haldane, Phys. Rev. B **53**, 15845 (1996).
- ³² K. Moon *et al.*, Phys. Rev. Lett. **71**, 4381 (1993).
- ³³ C. L. Kane and M. P. A. Fisher, Phys. Rev. B **46**, 15233 (1992).

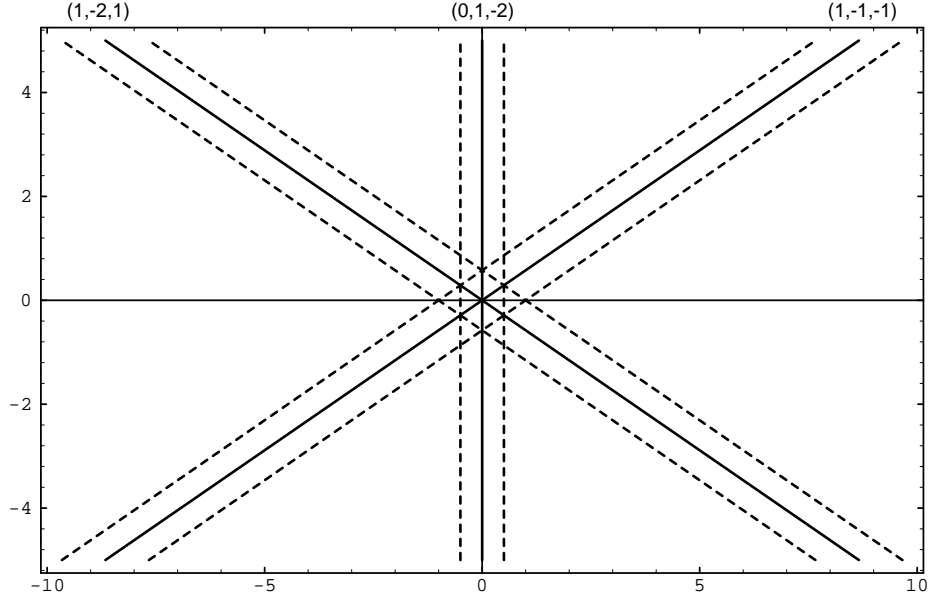


FIG. 1. Plot of scaling dimension of the three $|K(\mathbf{m})| = 2$ operators for $\nu = 3/5$ edge as functions of boost parameters (p_1, p_2) . The charge-unmixed point is the origin. Dashed lines indicate when operators become marginal ($\Delta(\mathbf{m}) = 3/2$) and solid lines indicate when operators become maximally relevant ($\Delta(\mathbf{m}) = 1$).

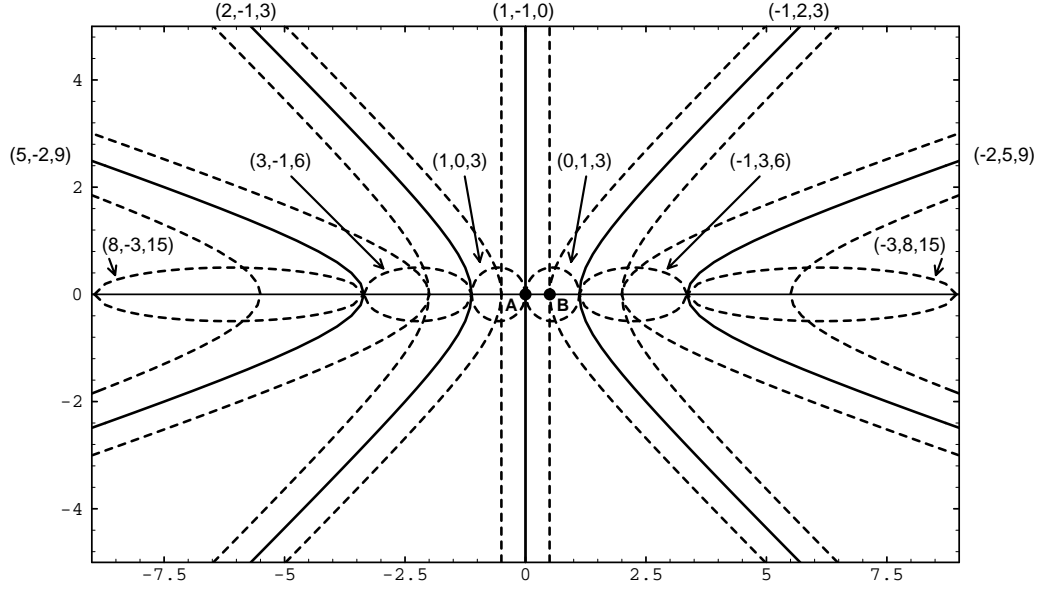


FIG. 2. Plot of scaling dimension of the first 11 $|K(\mathbf{m})| = 2$ operators for $\nu = 5/3$ edge as functions of boost parameters (p_n, p_c) . Dashed and solid lines are as in Fig. 1. The charge-unmixed line is the x -axis. At each point on the x -axis where one operator is maximally relevant, two other operators are marginal. Points A and B are examples of the two different types of fixed point.

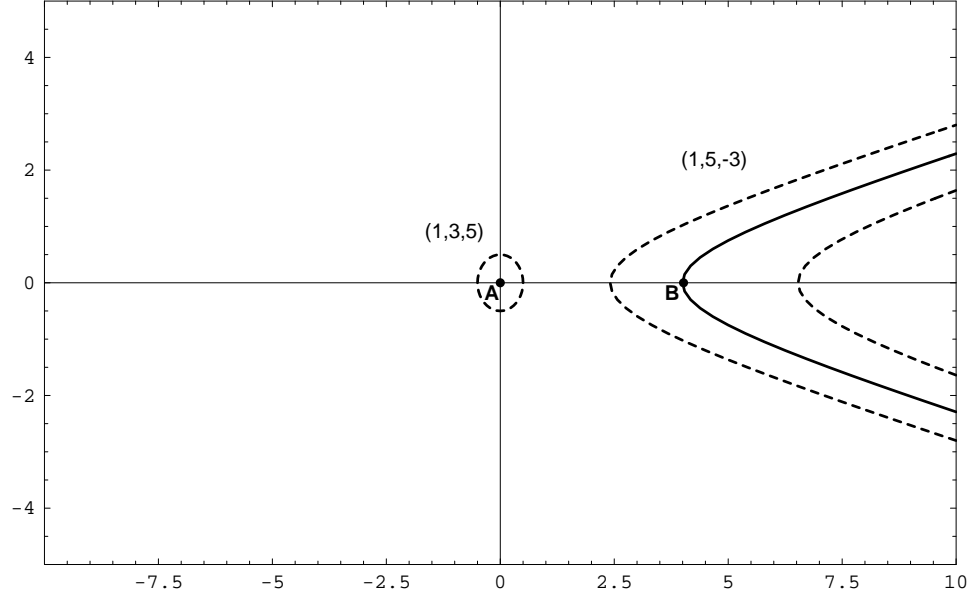


FIG. 3. Plot of scaling dimension of the two $|K(\mathbf{m})| = 2$ operators for $\nu = 17/13$. Axes are as in Fig. 2. At most points on the charge-unmixed line, there are no relevant disorder operators. Points A and B are the two charge-unmixed fixed points.

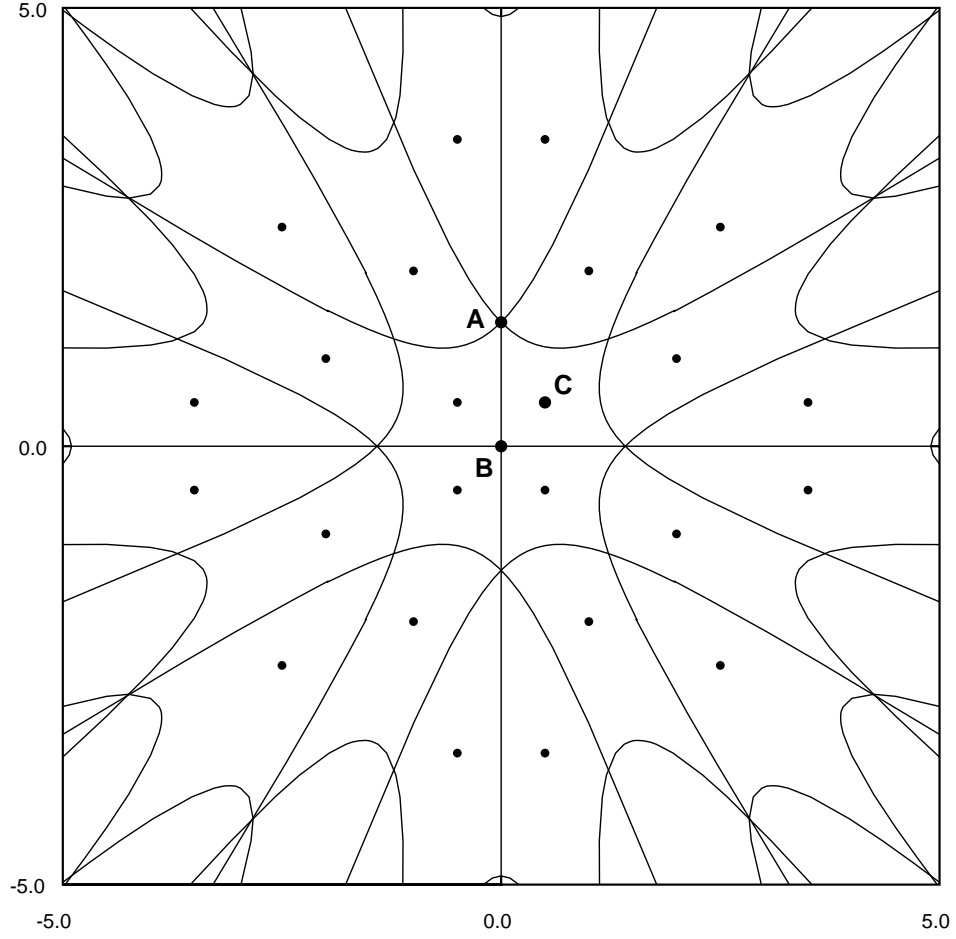
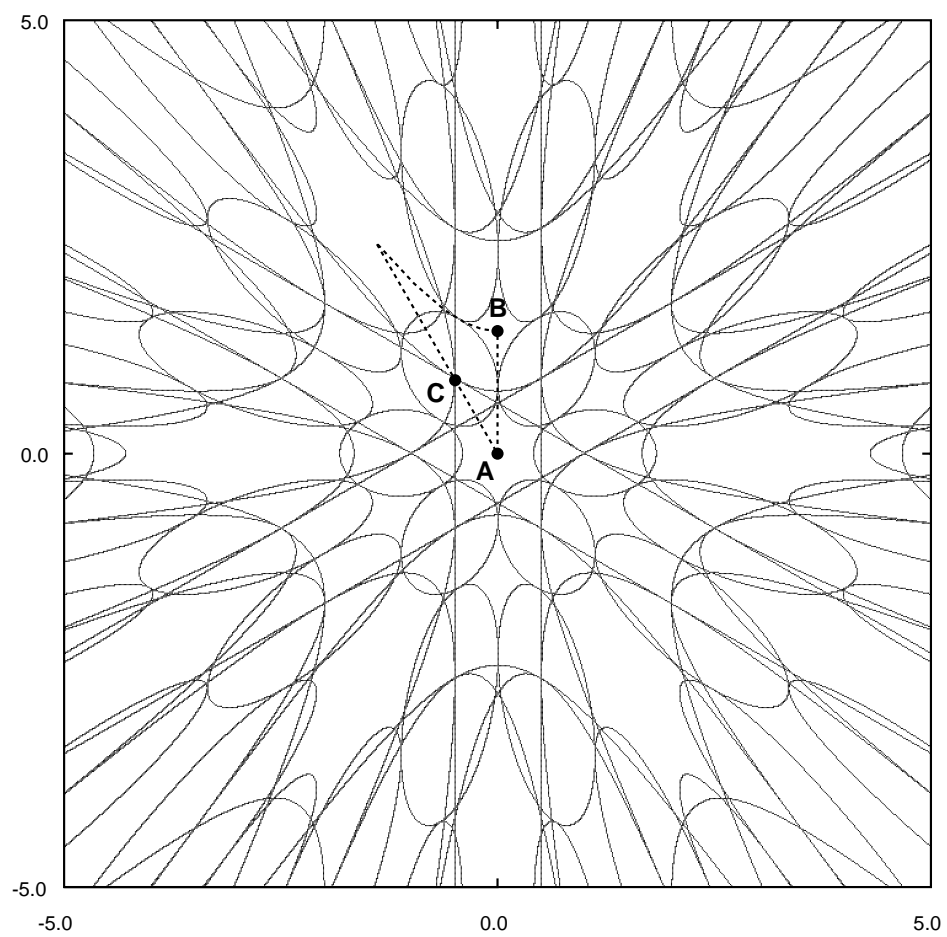
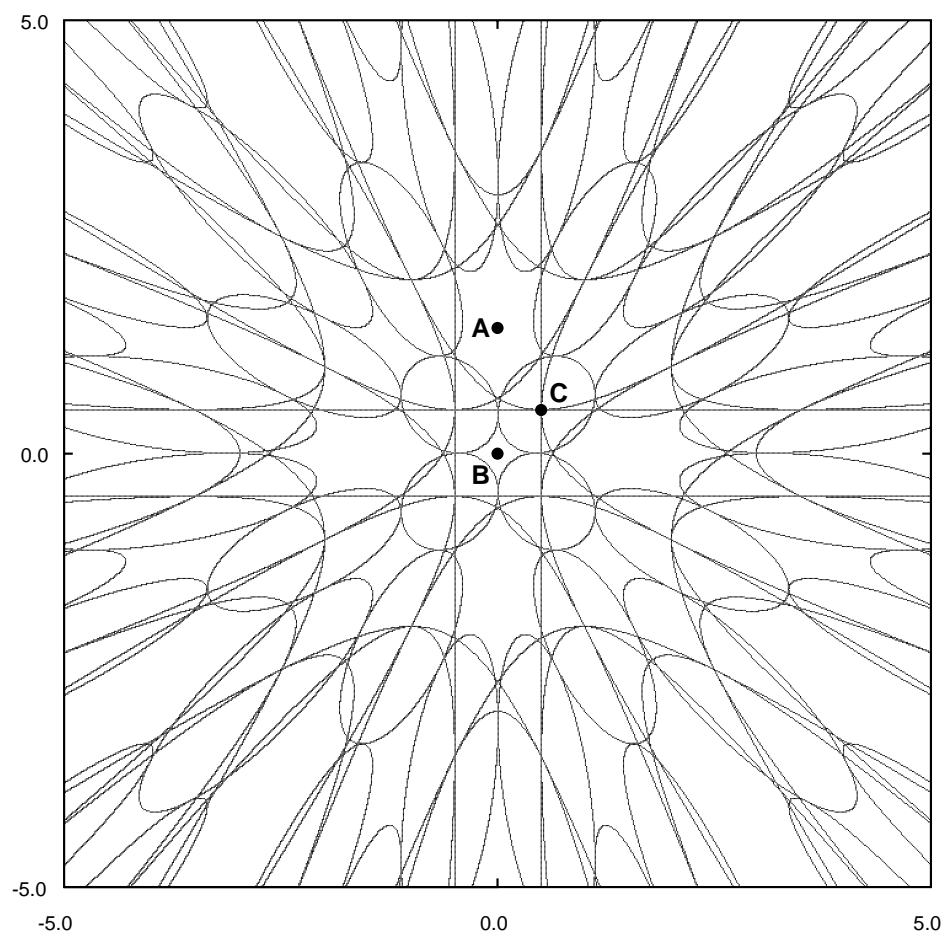


FIG. 4. The most relevant contours of $|K(\mathbf{m})| = 2$ operators on the charge-unmixed plane of the $\nu = 12/17$ edge as functions of boost parameters (p_1, p_2) . Points A, B, C are examples of the three different types of fixed points: A is an $SU(3)$ point, B an $SU(2) \times SU(2)$ point, and C a “double marginal” point. Dots are most relevant points of $K(\mathbf{m}) = 2$ operators, lines are most relevant lines of $K(\mathbf{m}) = -2$ operators.





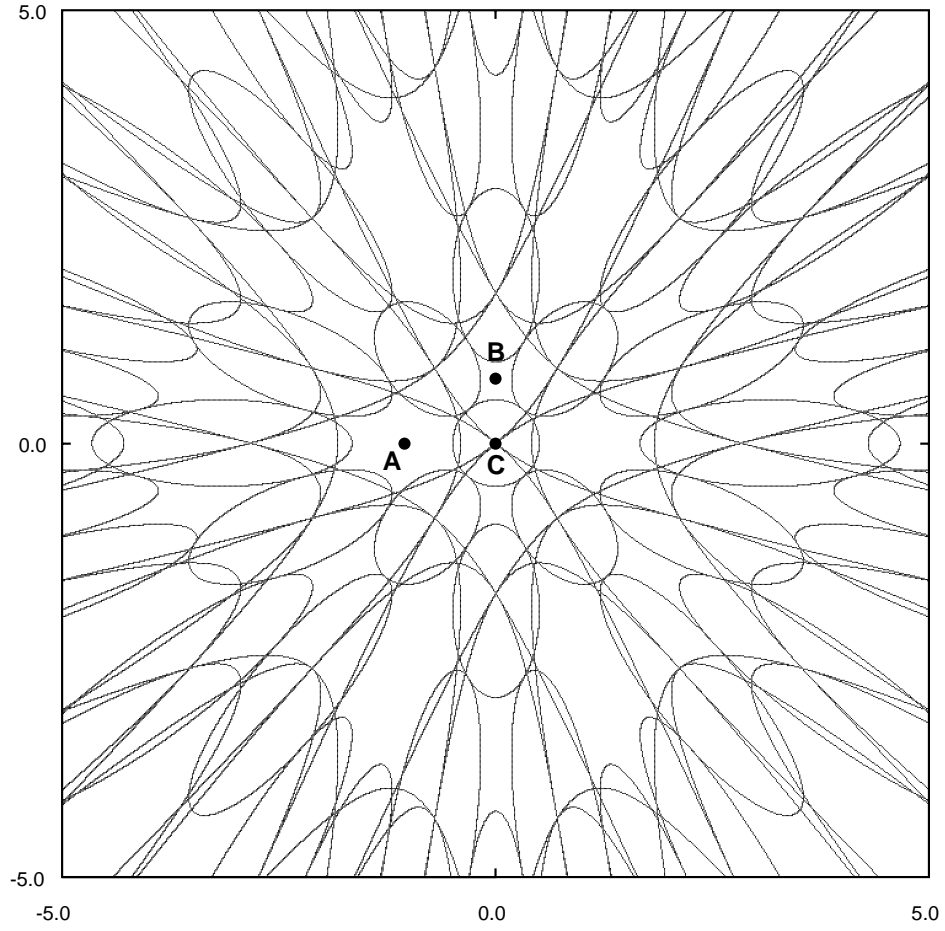


FIG. 5. Plots (a-c) show the *marginal* contours rather than the most relevant contours of $|K(\mathbf{m})| = 2$ operators for the $\nu = 12/17$ edge. The three plots were obtained using different bases: (a) has the $SU(3)$ point A at the origin and (b) the $SU(2) \times SU(2)$ point B , while (c) has the “double marginal” point C . Note that the three plots have the same topology. Plot (b) is the same as Fig. 4 except that marginal rather than most relevant contours are shown.

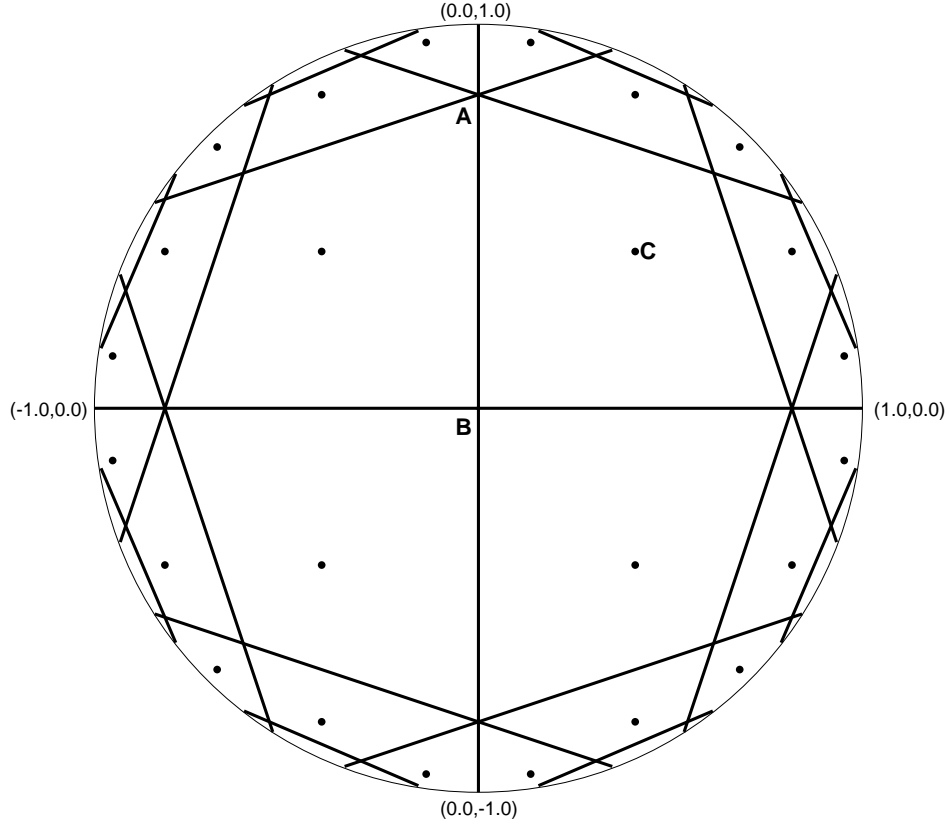


FIG. 6. The most relevant contours of $|K(\mathbf{m})| = 2$ operators on the charge-unmixed plane of the $\nu = 12/17$ edge as functions of “velocity” coordinates (v_1, v_2) . Plot is the same as Fig. 4 except that contours are shown as functions of “velocities” rather than “momenta”. Only the 42 most relevant operators at the origin are shown because the full diagram becomes infinitely dense at the edge of the circle.

TABLE I. Possible nonchiral edge types for $\dim K \leq 4$. For $\dim K = 5$ there are no principal hierarchy states and for $\dim K > 5$ no states at all which are T -stable and have neutral modes in both directions.

dim K	Mode directions (charge always \rightarrow)	Example	Boost parameters	Boost parameters with charge mode unmixed
2	$\begin{smallmatrix} 1\rightarrow \\ 1\leftarrow \end{smallmatrix}$	$\nu = 2/3$	1	0
3	$\begin{smallmatrix} 2\rightarrow \\ 1\leftarrow \end{smallmatrix}$	$\nu = 5/3$	2	1
	$\begin{smallmatrix} 1\rightarrow \\ 2\leftarrow \end{smallmatrix}$	$\nu = 3/5$	2	0
4	$\begin{smallmatrix} 3\rightarrow \\ 1\leftarrow \end{smallmatrix}$	$\nu = 12/31$	3	2
	$\begin{smallmatrix} 2\rightarrow \\ 2\leftarrow \end{smallmatrix}$	$\nu = 12/17$	4	2
	$\begin{smallmatrix} 1\rightarrow \\ 3\rightarrow \end{smallmatrix}$	$\nu = 4/7$	3	0

TABLE II. Low-temperature tunneling conductance behavior $G \sim T^\alpha$ for hierarchical daughter states of $\nu = 1$ (top) and $\nu = 1/3$. Only “charge-unmixed” phases (those with quantized conductance, or alternately those which can occur with long-range interactions) are shown. The different fixed points A and B for the Fibonacci-type states correspond to the labeling in Fig. 2. The phases $\nu = 12/7, 12/17, 12/31, 12/41$ have fixed lines L and three types of fixed point with $SU(2) \times SU(2)$ symmetry (abbreviated $SU(2)$ in the table), $SU(3)$ symmetry, or two independent marginal operators (DM). The tunneling exponent on the fixed lines L is nonuniversal. Note that each exponent in the lower table is given by $\alpha_{1/3} = 4 + \alpha_1$ where α_1 is the exponent of the state in the upper table. The pattern continues to lower filling fractions: daughter states of $\nu = 1/5$ have filling fractions between $1/8 < \nu < 1/4$ and tunneling exponents $8 \leq \alpha \leq 12$, e.g.

